

**Design, Simulation and Performance Analysis of an Educational Cosmic Ray
Muon Spectrometer**

Robin de Vos & Quinten L. Meeuwesen

Minkema college - Department of physics

PWS

Niels Bosboom

13-02-2026

© 2026 Robin de Vos & Quinten L. Meeuwesen

*This work is licensed under a Creative Commons
Attribution-NonCommercial-ShareAlike
4.0 International License (CC BY-NC-SA 4.0).*

*You are free to share and adapt this work for non-commercial purposes,
provided you give appropriate credit and distribute under the same license.*

<https://creativecommons.org/licenses/by-nc-sa/4.0/>

Abstract

In this paper, we challenge the issue of engineering an affordable yet precise cosmic muon spectrometer aimed at an educational audience, offering a fresh look on muon properties. We are leveraging the excitation properties of muon particles, by utilising a scintillator-based detector, that has an Onsemi MICROFC-60035-SMT SiPM sensor fixed at each corner of the plate. Using an AMD Artix™ 7 FPGA we can perform a TOF-measurement and using χ^2 -minimisation we can reconstruct the original trajectory, along with calculating other properties of the muon. To test the workings of our detector, we theoretically simulated the detector using Geant4—a simulation toolkit created by CERN, that is used to simulate the passage of radiation through matter—which yielded a hit accuracy of 2.32 cm and a theoretical timing resolution of 355 ps .

“One of the basic rules of the universe is that nothing is perfect. Perfection simply doesn’t exist ... Without imperfection neither you nor I would exist.”

-Stephen Hawking

Preface

Dear reader,

We are truly ecstatic to present the research paper called: “*Design, Simulation and Performance Analysis of an Educational Cosmic Ray Muon Spectrometer*”. This research paper is written with the aim to improve the quality of particle physics classes and theoretical physics education. We aim to provide a way of “seeing” the subatomic particles, which are merely mathematically defined in regular physics lectures. We strive to spark more interest among high school and college students who are not yet familiar with the subject matter. We believe that all people deserve to understand our universe in a sufficient way, either in a mathematical or a physical sense.

We are Robin de Vos and Quinten Meeuwesen, and we study a science based set of classes at Minkema College. This paper represents our final research project, or “profielwerkstuk, PWS” in Dutch, of our high school career. It was an incredible ride to dive so immensely deep into the material and finding out more about the world of particle physics, quantum mechanics and relativity. Not only did we delve into the theoretical aspect of the matter, we also indulged ourselves in the space of engineering an accurate detector. We believe we put our heart and soul into this, and we are incredibly proud of what we achieved as mere 17-year-old high school students.

To sum up, we want to acknowledge our accompanist, Mr. Bosboom, he has been a great help in forming our project and providing us with funding for practical research which we carried out. We also want to thank NIKHEF for providing us with a background into the subject and showing us already made cosmic muon detectors. Another party who was of great help was the Cosmic Watch project by MIT. Even though we did not directly converse with the creators of the Cosmic Watch, we were able to take in a lot of information and background provided by their earlier efforts.

*Robin de Vos & Quinten Meeuwesen
Woerden, 13 Februari 2026*

Contents

I Theoretical beauty of the universe	10
1 Introduction	11
1.1 Prior work	11
2 Theoretical framework	12
2.1 Cosmic rays	12
2.1.1 Muon flux	13
2.2 Muons in and of itself	13
2.3 Muons in cosmic rays	13
2.3.1 Relative muons	14
2.4 Muon interactions	15
2.4.1 Wave-particle duality	16
2.5 Detecting muons	16
2.5.1 Muon drift tubes (MDT)	16
2.5.2 Photomultiplier tubes (PMT)	17
2.5.3 Silicon photomultipliers (SiPM)	17
2.5.4 Cathode strip chambers (CSC)	18
II Detecting the undetectable	20
3 Design analysis	21
3.1 Prior work	21
3.2 Design goals and requirements	21
3.3 Detection method	22
3.4 Hardware component analysis	22
3.4.1 Detector plate construction	22
3.4.2 Microcontroller selection	23
3.4.3 Timing circuitry	23
3.4.4 Power supply	23
3.5 Signal processing and electronics design requirements	24
3.5.1 Raw SiPM Signal processing	24
3.5.2 Electrical noise	24
3.6 Detector noise	24
3.6.1 Multiple scattering	24
3.6.2 Energy loss	25
3.6.3 Error due to timing intervals	26
3.6.4 Theoretical resolution	26
4 Detector design	28
4.1 System overview	28
4.1.1 Operating principles	28
4.2 Detector assembly	28
4.2.1 Detector plates	28
4.2.2 Mainboard	29
4.2.3 Housing construction	30

4.3 Electronic components	30
4.3.1 SiPM Selection	30
4.3.2 Connecting the SiPM's to the mainboard	32
4.3.3 Timing equipment	32
4.3.4 Signal amplification and capturing	33
4.3.5 Signal measuring	34
4.4 Electrical circuitry	35
4.4.1 Design methodology	35
4.4.2 Power management	36
4.4.3 ADC	36
4.4.4 Amplifying and Peak Detecting circuits	37
4.4.5 FPGA Interface	37
4.5 Data processing	38
4.5.1 Measuring muon impact	38
4.5.2 Reconstructing the muon's trajectory	40
4.6 Quantifying our detector	41
4.6.1 Running the simulation	42
4.6.2 Simulating the cosmic ray	42
4.6.3 Simulating the detector	42
4.6.4 Defining the physical processes	44
4.6.5 Executing the simulation	44
4.6.6 Results	44
4.7 Calculating the properties of the muon	47
4.8 User interface	47
4.9 Cost estimates	48
III The end of a chapter	50
5 Conclusion	51
5.1 Our approach	51
5.2 Findings	51
5.3 Significance	51
6 Discussion	52
6.1 Interpretation of results	52
6.2 Design goals	52
6.3 Limitations	52
6.4 Further research	53
6.5 Comparison	53
6.6 Applications	53
6.7 Reflection	54
References	56

IV Appendices	60
Appendix A	61
A Special relativity	61
A.1 Mass-energy relation	61
A.2 Lorentzfactor	61
A.3 Characteristics of the Lorentzfactor	63
A.4 Conclusion	63
A.5 References	63
Appendix B	64
B Cosmic Watch	64
B.1 Principle of operation	64
B.2 Scintillator and photon detection	64
B.3 Amplifying, Triggering and Peak Detecting circuits	65
B.4 Event cycle	66
B.5 Other circuits	66
B.5.1 DC-DC Booster	66
B.6 References	67
Appendix C	68
C Muon trajectory detectors	68
C.1 Principle of operation	68
C.2 References	68
Appendix D	69
Appendix E	70
E Schematic BOM	70

I

Theoretical beauty of the universe

Design, Simulation and Performance Analysis of an Educational Cosmic Ray Muon Spectrometer

Robin de Vos & Quinten L. Meeuwesen

Minkema College - Department of physics - students

Muon spectroscopy is utilized in a wide variety of scenarios and situations, but how does such a machine work precisely? And how can it be made? We will analyse this in this paper.

1 Introduction

Since the dawn of time, humanity has asked itself two seemingly simple questions, “*Where do we come from?*” and “*How did it all begin?*” These questions, however, are not so simple after all. Nevertheless, there are ways of providing explanations for these questions. Research into cosmic rays provides us with these.

Cosmic rays are beams of elementary particles originating from black holes, supernovae and other intergalactic processes. These rays offer insight into these galactic activities.

Because the inter-celestial bodies in the universe are so far apart, it will take the particles an incredible amount of time to arrive on earth; this can go up to 13.5 billion years ago.

Cosmic rays consist of plenty of particles. By measuring the velocity and other properties of these particles, you can calculate where the particles originate from and how much energy they transport, which can give us insights into our universe and how it originated. Measuring these particles—muons in particular—is a difficult feat, but we will try to conquer this in this paper. The largest amount of particles in these cosmic rays are muons, thus are most optimal to measure. This is why we arrive at the following research goal.

Our goal in this paper and project is to theoretically engineer a working muon spectrometer, which is able to be used for educational purposes.

Research in this field is available, but there is not much information about a spectrometer that calculates interesting properties, such as speed, track and momentum, for an educational environment. These types of measurements are only made by institutions like universities and CERN for professional research.

Our goal for this paper and project is to engineer a working muon spectrometer, which is able to be used by non-physics-institutes for educational purposes and giving more of an insight into particle physics and cosmic processes for high schools and other non-physics-institutes.

We strive to make the muon spectrometer easier to use than existing solutions yet remain sophisticated. And thus provide a way of teaching and analysing the interesting insights into the difficult structure of the field of particle physics without fully understanding the challenging mathematical structure.

1.1 Prior work

Some previous efforts have been made to make muon detectors more accessible. One example is the Cosmic Watch project created by MIT. They aimed to make a desktop muon

detector that is easy and cost-effective to make.

Although this device is very simple to make and use, we would like to try and make something more sophisticated, as to actually provide us with some useful information about the muon, instead of only that there is a muon.

A group of students at the University of Exeter have also tried to develop a similar detector, but that one does have the capabilities to also detect other information, like the direction of the muon. But as far as we know, the project has never been finished.

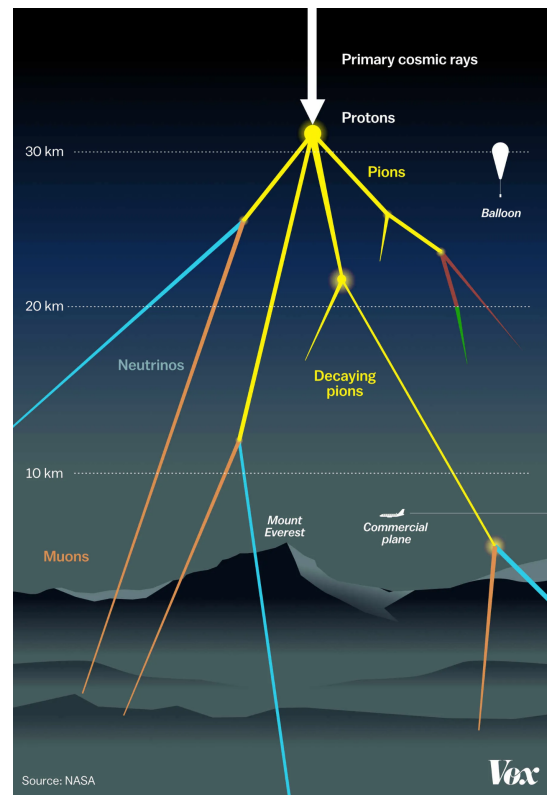


Figure 1: Schematic view of a cosmic ray originating from space. (Source: [\[11\]](#))

2 Theoretical framework

Cosmic rays pass through earth and even through our body every second. But what are these rays even? And how do they work? We will discuss this in this chapter.

2.1 Cosmic rays

A cosmic ray is a set of particles produced in numerous astrophysical processes, such as merging black holes, exploding stars (supernovae), or even solar storms from our own sun.

When a proton or any other particle is emitted from one of the aforementioned processes, it travels at nearly the same speed as light. This means that the particle must have an extremely high amount of energy. When the particle collides with our atmosphere, it undergoes an interaction with the particles in the atmosphere, resulting in a cascading avalanche of particles. One of the particles that originates from these collisions is the negatively charged pion (π^-), which in turn can decay to the muon according to the equation below. [\[2\]](#)

$$\pi^- \rightarrow \mu^- + \nu_\mu \quad (1)$$

These muons, which are produced in the cosmic showers, are emitted throughout the entire atmosphere. The relative abundances of the radiation in the atmosphere at different altitudes, with the particles having at least 1 GeV of energy, are illustrated in Figure 2. As can be seen in the figure, most muons are produced at an altitude of $\sim 15\text{ km}$. This is where the high-energy collisions take place.

2.1.1 Muon flux

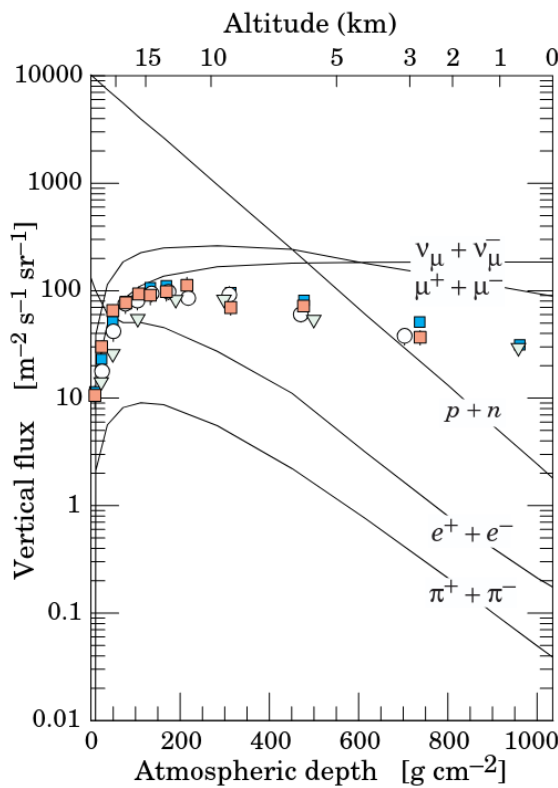


Figure 2: Vertical fluxes of cosmic rays in the atmosphere, with the particles having at least $E = 1 \text{ GeV}$. The points show measurements of negative muons at the given altitude. The lines show the correlation between the altitude and vertical flux of the labelled particles. (Source: [2])

The amount of particles that reach the earth per square meter at any given second, can be defined as the vertical flux. For muons, it is about $100 \text{ m}^{-2} \text{ s}^{-1} \text{ sr}^{-1}$. Here, sr is a steradian, which is the three-dimensional equivalent of the radian, so a three-dimensional angle.

However, for the purposes of our analysis, this can be neglected for now. We will use a vertical flux of $100 \text{ m}^{-2} \text{ s}^{-1}$ coming roughly from the upwards direction.

2.2 Muons in and of itself

The muon (μ) is a charged elementary particle, similar to the electron. It belongs to the second generation of leptons according to the standard model of elementary particles. This means that the muon shares a lot of the same

properties as the regular electron, like its spin ($1/2$) and electrical charge (-1). With the main difference between the electron and muon being its mass and lifetime. A muon is about 200 times heavier than the electron, a muons mass is approximately $105.66 \text{ MeV C}^{-2}$ [1]. The muon and antimuon decay through the weak interaction, resulting in two species of neutrinos, electrons and positrons. This decay can be described by the following equations. [2]

$$\mu^- \rightarrow e^- + \bar{\nu}_e + \nu_\mu \quad (2a)$$

$$\mu^+ \rightarrow e^+ + \bar{\nu}_\mu + \nu_e \quad (2b)$$

This decay can be further defined by the lifetime of a muon, $\tau_\mu = 2.2 \mu\text{s}$ [2].

2.3 Muons in cosmic rays

Even though a muon's lifetime is only $2 \mu\text{s}$, it will still travel further than light would in 2 microseconds. But how is that possible? A particle is physically restricted to travel faster than the speed of light. This is a proven statement, but there is something else at play; time dilation.

$$v = \frac{s}{t} \quad (3)$$

This equation [1] explains the speed an object has over a certain distance with respect to the time it took. If we apply this to our muon, with a distance of at least 15 km, as the average height of muon production is at $\sim 15 \text{ km}$ above sea level. [^2.1] And travels down to at least sea level. And we take a simplified mean lifetime of the muon, τ_μ , as the travel time, we would get the following velocity.

$$v = \frac{h}{\tau_\mu} = \frac{15 \cdot 10^3}{2 \cdot 10^{-6}} = 7.5 \cdot 10^9 \text{ m s}^{-1}$$

The speed of light is defined as $c = 2.998 \cdot 10^8 \text{ m s}^{-1}$ [1]. So according to

Newtonian mechanics, our muon travels faster than light, which is physically impossible due to Einstein's theory of relativity.

This is because an object travelling close to the speed of light experiences time dilation. When an object experiences this phenomenon, time appears to be moving slower from the perspective of another observer compared to the moving object's own perception.

So, the time that a muon “lives” appears to be longer than the mean lifetime of the muon from the perspective of a static reference frame. However, when moving alongside the muon, the measured time actually is not greater than the mean lifetime. This is why it is important to take relative physics into account, because by accounting for time dilation we can attain the correct time measurement and thus get the correct speed.

In order to take time dilation and other relative processes into account in various formulas, we use something called the Lorentzfactor, γ , which is defined as the following. [1]

$$\gamma = \frac{1}{\sqrt{1 - (\frac{v}{c})^2}} \quad (4)$$

The behaviour of this formula, is that when v approaches the speed of light, the Lorentzfactor approaches infinity.

This may sound a bit confusing at first, but it actually is not all that difficult to understand. A longer, more in depth explanation, as well as the full derivation of the Lorentzfactor can be found in Appendix A.

2.3.1 Relative muons

In order to calculate the actual relativistic speed of a muon arriving on earth, we must start with rewriting the equation for the Lorentzfactor (4) to the velocity as a function of the Lorentzfactor, giving us the following.

$$\gamma = \frac{1}{\sqrt{1 - (\frac{v}{c})^2}}$$

$$\frac{1}{\gamma} = \sqrt{1 - (\frac{v}{c})^2}$$

$$\frac{1}{\gamma^2} = 1 - (\frac{v}{c})^2$$

$$(\frac{v}{c})^2 = 1 - \frac{1}{\gamma^2}$$

$$\frac{v}{c} = \sqrt{1 - \frac{1}{\gamma^2}} \quad (5)$$

We start by defining the fractional v/c as a function of the Lorentzfactor, where the Lorentzfactor is a scale for the amount of time dilation a particle experiences. Plotting (5) on a graph, we can observe that the larger γ gets, the more the particle approaches the speed of light. (Figure 3)

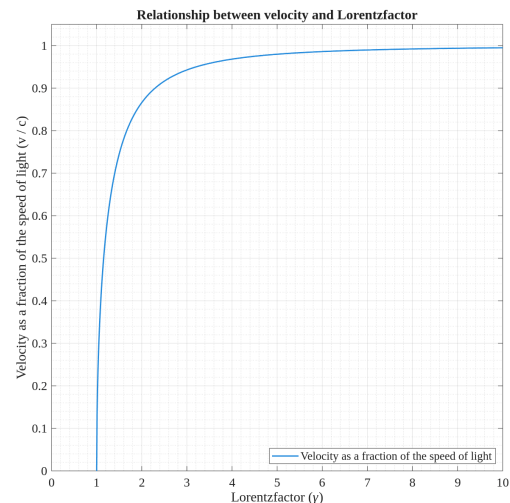


Figure 3: Relationship between velocity and Lorentzfactor.

The unit on the y-axis is the fractional v/c . We have chosen this to better visualize the velocity approaching the speed of light, as if $v/c = 1$ means $v = c$.

If we get rid of the fractional in (5) we get the actual equation for the velocity as a function of the Lorentzfactor.

$$v = c \sqrt{1 - \frac{1}{\gamma^2}} \quad (6)$$

Speed is classically defined by (3). In order to get the correct velocity we use the time

measurement from the reference frame on earth which can be defined as the mean lifetime of the muon times the Lorentzfactor to account for relativity, as can be seen in Appendix A. Using this relation, we derive the following equation.

$$t_{\oplus} = \gamma \tau_{\mu} \quad (7)$$

With t_{\oplus} being externally measured time on earth and τ_0 the mean lifetime of the muon. If we substitute (7) into (3) and rewrite for γ we get the equation below.

$$v = \frac{s}{t}$$

$$v = \frac{s}{\gamma \tau_{\mu}}$$

$$s = v \gamma \tau_{\mu}$$

$$\gamma = \frac{s}{v \tau_{\mu}} \quad (8)$$

Because we are observing ultra-relativistic cosmic rays ($\gamma \gg 1$), the speed of the muon satisfies $v \approx c$, therefore we set $v \simeq c$ in our equation. Due to the speed of the designated muon being so close to the speed of light, we get approximately the same Lorentzfactor. So substituting v for c we get (9'). In addition to this we can assume a situation where a muon is produced perpendicular above the measurement installation, thus resulting in $s = h$, where h is the height of muon production, we get (9).

$$\gamma = \frac{s}{c \tau_0} \quad (9')$$

$$\gamma = \frac{h}{c \tau_0} \quad (9)$$

We derive our relativistic speed formula by substituting (9) into (6), resulting in (10).

$$v_{\mu} = c \sqrt{1 - \frac{1}{(\frac{h}{c \tau_0})^2}} \quad (10)$$

This equation shows the relation between the height at which a particle is produced and the minimum speed it needs in order to travel back to earth, accounting for relativity. If we plot this relation and the relation between the height and the Lorentzfactor (9) we get the following graph.

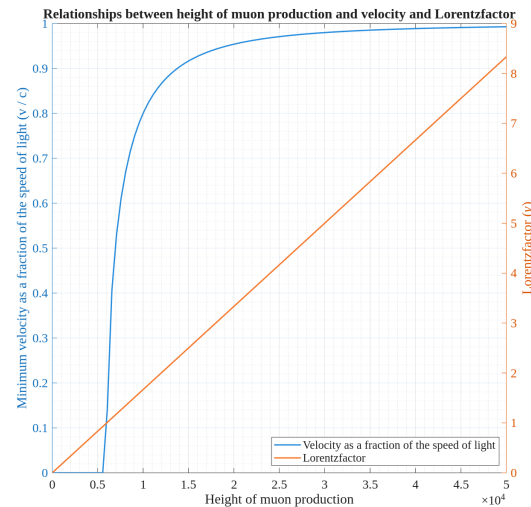


Figure 4: Relationships between the height of muon production and velocity and Lorentzfactor.

In this graph we can see that the higher a muon is produced, the higher the Lorentzfactor is and thus the faster it travels down to earth. This proves that muons undergo relativistic effects and thus are able to reach the ground before decaying even though classical mechanics says otherwise.

2.4 Muon interactions

Similarly to neutrinos, muons react with almost no other matter, meaning they can travel through large amounts of rock and still remain intact. However, unlike neutrinos, muons can experience scintillation and ionization, which can be used to reliably detect muons.

Scintillation is an example of luminescence, where a scintillator material becomes luminescent when exposed to ionizing radiation, such as muons. [3] When a material becomes luminescent, it emits photons, which in turn can be detected.

A different way of detecting muons is by leveraging a special gas mixture that gets ionized when struck by ionizing radiation. This ionization releases electrons, which can then also be detected.

2.4.1 Wave-particle duality

If the emitted photons described in the previous section were to behave as particles, we would have a very difficult time detecting them, as the photon particles would just drift in a random direction, with a minuscule chance of actually hitting the detector.

This is where one of the special properties of the photon is used, its wave-particle duality. [4] Wave-particle duality is a concept in quantum mechanics where a particle can exhibit both particle and wave characteristics. At any given moment, the particle acts as both a particle and a wave. However, when we try to measure a state property of the photon, this duality state collapses, and it behaves as either a particle or a wave. Although this concept is quite strange and difficult to understand, only a very primitive knowledge of this concept is required to understand our detection methods.

Given a scintillator material as an example, when a muon strikes the material, a photon is emitted at the location of impact. The wave property of the photon will radially propagate outwards from the impact location, but when we try to measure the photon—when it hits a detector—the duality will collapse, and thus behave as a single particle, which we can detect.

2.5 Detecting muons

There are plenty of ways to measure the presence of muons, but most of them work based on the same working principles. They make use of the two interaction principles described earlier, either ionization or scintillation.

Below, we will explain four of the most commonly used methods for measuring muons.

2.5.1 Muon drift tubes (MDT)

Muon drift tubes (MDT) are one of the most widely used forms of detecting muons, known for their accuracy and cost-effectiveness. This is why they were chosen for muon detectors in the ATLAS detector in the Large Hadron Collider at CERN.

The construction of MDT's are relatively simple, they consist of some sort of tube or hollow space with a small anode wire through the centre and some cathode strips at the sides of the tube. This tube is then filled with a certain gas and a small electric current is applied to the anode and cathodes to create an electric field. [5] (Figure 5)

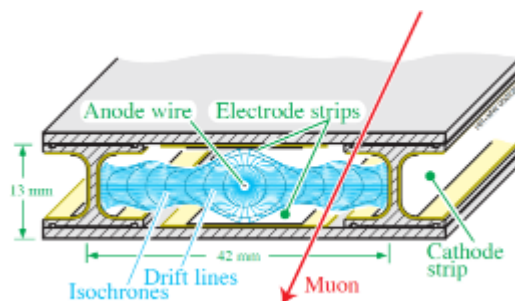


Figure 5: Schematic view of a muon drift tube used inside the ALAS detector at CERN. (Source: [7])

When a muon passes through this tube, the muon ionizes the gas inside the tube, creating free electrons. These electrons then move ('drift') toward the central anode wire, guided by the electric field, and when they reach the wire, they can be measured. Because the drift velocity of the electrons is nearly constant, the time it takes the electrons to reach the anode wire can be used to calculate the distance the electrons travelled from their original atoms. [6]

To measure the precise path of the muon, the tubes can be arranged in a grid, consisting of multiple layers. Because each grid can only measure the path in one dimension, multiple grids are placed on top of each other with

different orientations to be able to calculate the precise 3D path the muon travelled.

MDT's are almost always used in combination with another form of detecting muons. This other detector is used as a trigger to be able to calculate the drift time, which in turn allows calculating the drift distance inside the MDT's.

2.5.2 Photomultiplier tubes (PMT)

Photomultiplier tubes (PMT) are extremely sensitive photon detectors. However, they cannot measure muons directly, instead they are used in conjunction with a scintillator.

Photomultiplier tubes are typically created from a vacuum pumped tube. A photocathode is placed on one side, a number of electrodes, called dynodes, in the middle and an anode is placed on the other side. An electric current is applied to the electrodes such that each dynode is held at a more positive potential than the previous one, so the further from the cathode, the higher the positive potential on the dynodes. (Figure 6)

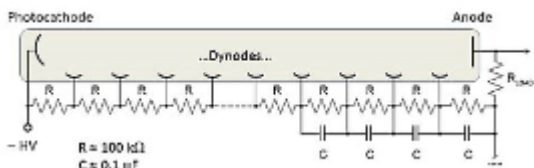


Figure 6: Schematic view of a photomultiplier tube, where each dynode is held at a more positive potential than the previous one, regulated by the resistors between each dynode. (Source: [8])

When the photocathode is struck by a photon, it releases a free electron towards the first dynode. Upon reaching the first dynode, more electrons are emitted, a process which is called secondary emission. The dynodes are placed in such a way that the electrons from the secondary emission accelerate towards the next dynode. This process repeats itself a couple of times, until they reach the final anode. When the electrons reach the anode, the amount of electrons has grown significantly, such that they create a

measurable current pulse, 50 ns after the photon hits the photocathode, that is easily detectable. [6] (Figure 7)

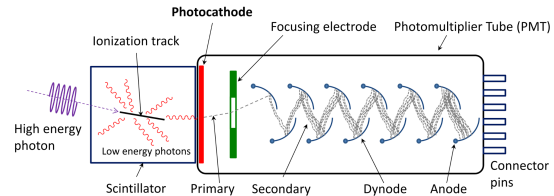


Figure 7: Schematic view of a photomultiplier where the path of the electrons is traced. (Source: [8])

Because PMT's are so fast, they are typically used as the trigger for a system using MDT's [^2.5.1], to be able to accurately calculate the muon's trajectory.

2.5.3 Silicon photomultipliers (SiPM)

In more modern systems, silicon photomultipliers (SiPM) have superseded the more traditional photomultiplier tubes, because of their numerous benefits, notably that they are more deterministic, suffering much less from noise, and much easier to mass produce, which in turn allows them to be made cheaper. [9]

SiPM's operate based on the same principle as traditional PMT's, as in that they create a free electron from a photon, which creates a chain reaction that results in sometimes millions of electrons. But the way that they do this is a lot different.

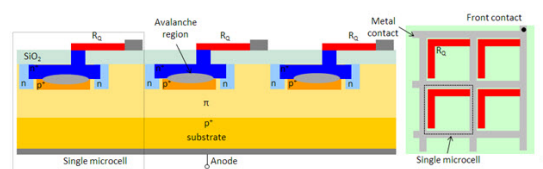


Figure 8: Schematic of the structure of a typical silicon photomultiplier (side & top view). (Source: [9])

A SiPM is constructed from a large grid of microcells, each containing a single-photon avalanche diode (SPAD), all sharing the same anode and cathode pins. A bias voltage (V_{bias})

is applied to the anode and cathode, which puts each diode in its Geiger mode and when the diode is struck by a single photon with enough energy, it discharges through the cathode. [9] (Figure 8)

To explain how a SiPM works, we will use an equivalent electrical circuit similar to how a SiPM actually works, as seen in Figure 9.

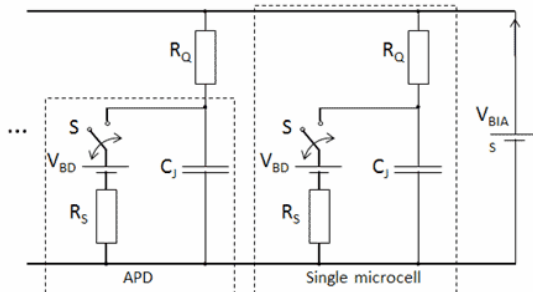


Figure 9: Schematic of an equivalent electrical circuit of two single-photon avalanche diodes inside a silicon photomultiplier. (Source: [9])

When there are no photons present, the switch S is closed, and the capacitor (C_j) is charged to V_{bias} . When the SiPM absorbs a photon, it creates an electron-hole pair, essentially this means that the photon's energy frees an electron from its silicon atom, leaving behind a positively charged 'hole', the silicon ion.

This electron then reaches the 'avalanche region', where an extremely strong electric field is present (the charged capacitor, C_j). Because of this electric field, the electron accelerates, gaining a lot of kinetic energy. When this electron crashes into other silicon atoms, they also release free electrons, creating more electron-hole pairs. This cascading effect is called the 'avalanche'.

While this process is taking place, the switch (S) closes, allowing the capacitor (C_j) to discharge. When the capacitor's voltage reaches the breakdown voltage (V_{BD}) the switch (S) closes again, allowing the capacitor to charge back up to V_{bias} , thus resetting the system.

In reality, the switch (S) is not really a switch, but rather the electrons that create a conducting path through the silicon, when the capacitor (C_j) discharges, the electric field weakens, slowing down the avalanche effect until it stops completely, which is when the capacitor reaches the breakdown voltage. When the avalanche effect stops, the conducting path of electrons also disappears, so the switch (S) 'closes'. [9]

The 'magic' of the SiPM is that each SPAD is in the so-called Geiger mode, essentially each diode is primed, and when even a single photon gets absorbed the avalanche takes place and the capacitor gets discharged. The discharging of the capacitor is what is measured to know when a photon has been absorbed by the SiPM.

2.5.4 Cathode strip chambers (CSC)

Cathode strip chambers (CSC) share some working characteristics from both MDT's and SiPM's, combining elements from both detection methods.

A single layer of a cathode strip chamber, consists of cathode strips on one side, anode wires running in the perpendicular direction in the middle and a cathode plate on the other side. The space between the two cathode plates is filled with a special gas mixture, similar to what is used in MDT's. [^2.5.1] (Figure 10)

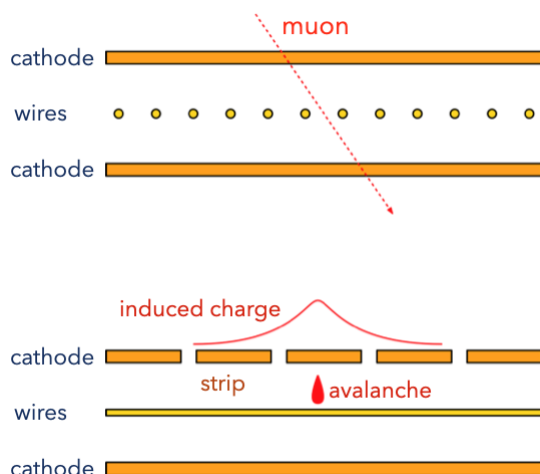


Figure 10: Schematic view of the construction of a cathode strip chamber, also showing the induced charge from a muon particle passing through. (Source: [10])

When a muon passes through a layer of the CSC, it ionizes the gas atoms, knocking electrons free. These electrons drift toward the anode wires, where the strong electric field causes avalanche multiplication, amplifying the signal, similarly to what happens in a SiPM. [^2.5.3] Meanwhile, the positively charged ions drift toward the cathode strips. As these charges move through the chamber, they induce measurable signals on both the cathode strips and the anode wires. [10]

Due to the perpendicular arrangement of the cathode strips and anode wires, the impact location of the muon can be determined in two dimensions: one coordinate is measured from the induced charge on the cathode strips, while the perpendicular coordinate is measured from the signal on the anode wires.

II

Detecting the undetectable

3 Design analysis

Now that we have a fundamental understanding of what muons are, where they come from, and how to detect them, we can start designing the working principles of our detector.

3.1 Prior work

While muon detection has traditionally been limited to large research institutions and particle physics laboratories, there have been growing efforts in recent years to make this technology accessible for educational purposes. Several projects have attempted, to varying degrees of success, to develop compact, affordable muon detectors that can be used in classroom settings or by citizen scientists, each with varying degrees of success and different capabilities.

By examining these existing solutions, we can identify proven approaches, as well as improving some of their shortcomings that our detector could address. Below, we will discuss the recent solutions that we think are good designs to base our detector off.

The first and most sophisticated consumer available muon detector is the Cosmic Watch. The Cosmic Watch is a desktop muon detector that originated from MIT. The most recent version has been developed by the University of Delaware. In order to get a good understanding of this device, we decided to make a detailed analysis of it, which is accessible in Appendix B.

In short, the device is a desktop Cosmic Watch aimed at educators, students and enthusiasts. It is capable of performing muon measurements as well as utilize a second detector to perform coincidence detection for more precise results. The detector uses a scintillator-based detector along with a SiPM sensor. (Appendix B)

Besides the Cosmic Watch, there have been a handful of other similar projects. While most

are similar to the Cosmic Watch in terms of functionality and measuring capabilities, two other projects that are worth noting are the detectors by students at the University of Exeter and by students at Texas A&M University. Both of these detectors are theoretically capable of measuring muon trajectories.

Since the workings of both of these detectors are so similar, we have created a single analysis that looks at both, this can be found in Appendix C. In short, the devices use two detector plates which are capable of measuring the impact location on the plates. They can then reconstruct a vector that fits between these two points, which is the muon's trajectory.

3.2 Design goals and requirements

Before we start designing our own detector, we need to lay out a few requirements that our detector should follow, as well as some goals and features that it should have.

Similarly to the Cosmic Watch, our detector should be suitable for educational and personal use, thus it should be relatively easy to use and perform maintenance on. This also means that the construction of the detector should be relatively compact and quite movable.

Besides measuring the mere existence of muons, our detector should also be capable of measuring more advanced properties of muons, such as trajectory and velocity. This will make for more interesting results and better demo's.

In order to actually visualize and calculate the collected information, we need to develop the foundational mathematics needed for using the detector. We also must provide the foundation of the accompanying software. Which must include tables and visualizations of the calculated trajectories and measurements.

And finally, to tie the whole package together, the hardware should use common parts and be easily accessible. The software should also be accessible and available to download. This will make it possible to build a detector yourself.

3.3 Detection method

Our prior research has yielded four possible detection methods, namely MDT, PMT, SiPM and CSC. [^2.5] However, several of these methods were immediately eliminated for practical reasons. MDT's and CSC's, while highly accurate and widely used in professional installations, require complex gas handling systems, complicated electronics and external triggering methods. These methods would be far too complex, and would not fit our requirements of being cost-effective and relatively compact, nor would it be suitable for educational or personal use. [^2.5.1, ^2.5.4]

Traditional photomultiplier tubes (PMT) require high operating voltages, typically in excess of 1000 V. This poses several safety concerns when used in an educational setting and would require complex high-voltage power supplies. [^2.5.2]

This leaves us with one method remaining: the Silicon photomultiplier (SiPM). SiPM's offer compelling advantages that make them extremely suitable for our application. Compared to PMT's, they operate at much lower voltages, typically around 25 – 75 V, which removes the safety concerns, as well as the need for high-voltage power supplies. SiPM's also do not require any gasses to work, instead, relying on a scintillator material [^2.4]. The required electronics are also relatively easy, and they do not need any external triggering mechanisms. [^2.5.3]

Modern SiPM's have excellent photon detection efficiency, providing reliable measurement while being less susceptible to

electromagnetic interference compared to other detection methods.

The success of the Cosmic Watch project, detailed in Appendix B, demonstrates that SiPM-based detectors can achieve meaningful muon measurements in an educational context. These advantages have also been noticed by other, similar, projects that have also leveraged SiPM's, they have even managed to extend the SiPM's capabilities in order to built pixel detectors. These detectors are capable of detecting the precise position of the muon's impact, which was previously only possible with CSC based detectors. Projects, such as the muon detectors from the University of Exeter and Texas A&M University, are primary examples. (Appendix C)

For practical reasons, a scintillator-based detection system in combination with a SiPM sensor is the only viable approach for our detector, as the other methods require more advanced circuitry or are not safe enough for an educational setting.

Because of these reasons, we have chosen to use a scintillator-based detection system in combination with a SiPM sensor for our detector. This combination offers the most suitable balance of performance, cost and practicality for an educational setting.

3.4 Hardware component analysis

Now that we know what kind of detector we are going to be making, we can start choosing what kind of components we are going to be using and what requirements they should have.

3.4.1 Detector plate construction

The detector plate is responsible for capturing the muon interactions and converting this to a signal that can be processed. As mentioned previously, we have chosen to build a

scintillator-based detector with a SiPM sensor.

[^3.3]

Firstly, the scintillator plate needs to be optically coupled to the SiPM sensor. This can be achieved by using an optical coupling compound. The optical coupling compound minimises light loss at the scintillator-SiPM interface and matches the refraction index of the scintillator material.

If we were to connect this construction to a detector, we would not get any clear information. As photons from the surrounding light will interfere with our measurements. That is why we have to optically isolate the detector plate from its surroundings.

This is done by wrapping the entire plate in aluminium foil, not only will this block ambient light, but it will also block other low energy radiation from exciting the scintillator. Finally, the plate is wrapped in a dark, isolating tape, such as black electrical tape. This will ensure that everything remains together and will block further light spill. When wrapping the plate, a small area is left unwrapped, as this is where the SiPM sensor interfaces with the scintillator plate.

This approach is similar to what was used in the Cosmic Watch and the University of Exeter. (Appendix B, C)

3.4.2 Microcontroller selection

The selection of the microcontroller is critical for ensuring reliable and accurate operation, thus it does have a few requirements.

Given an average vertical flux of $100 \text{ m}^{-2} \text{ s}^{-1}$ [^2.1.1], the microcontroller has to perform 100 measurements per second given a detector plate of 1 m^{-2} , which is very large. 100 measurements per second can easily be achieved by even some of the slowest microcontrollers available, thus the speed of the microcontroller does not actually matter that much in our selection.

One aspect that is important in the selection, is the requirements surrounding the analog to digital converter (ADC). The ADC is responsible for measuring the peak voltage, and it is thus important that this measurement is accurate.

For our purposes, we have chosen to require a minimum resolution of 12-bit. In practise, this means that the ADC can measure $2^{12} = 4096$ different analog levels. Given a typical operating voltage of 3.3 V for microcontrollers, our ADC is capable of measuring voltage increases of $3.3 / 4096 = 0.805 \text{ mV}$. In addition to the resolution, we should also have multiple channels available to allow performing more complex measurements, where we require more than one SiPM sensor. [12]

3.4.3 Timing circuitry

In order to perform advanced muon measurements, we have to precisely measure time differences between events. These measurements require different precision.

Timestamp measurement is useful for keeping track of when muon events have taken place, but these timestamps do not have to be super accurate; millisecond accuracy will suffice. This accuracy can easily be achieved using the microcontroller's built-in timing logic.

However, more complex measurements such as coincidence detection or building a pixel detector require far more accuracy, and this is when the microcontroller's timing logic will not keep up. A solution for this is to use field programmable gate arrays (FPGA's) these are high speed, programmable integrated circuits. [13]

3.4.4 Power supply

Not every component requires the same voltage. There are three prominent components that require a certain voltage, namely the SiPM, microcontroller and if necessary, op-amps.

The most difficult component is perhaps the SiPM, as it requires a high bias voltage, typically $\sim 30 - 70\text{ V}$. However, the SiPM does not consume a lot of current, therefore we can quite easily use a lower voltage that is suitable for the other components, and boost that voltage to the required bias voltage for the SiPM with some simple electronics.

Microcontrollers typically require 3.3 V or 5 V . However, we will most likely be using a microcontroller devboard for simplicity, which are almost always powered using a USB connector, thus inherently require 5 V .

The last active component is the op-amp. Although the voltage requirements of op-amps vary, the ones that we are most likely going to be using will match the 5 V of the microcontroller.

3.5 Signal processing and electronics design requirements

Building a muon detector with the thus far gathered knowledge, is not as simple as connecting the components together. We first have to process the signal coming from the SiPM, before we can actually do something with it. In addition to this, we also have to take into account that the voltage coming from the power supply will never be perfect, and thus contain background noise.

3.5.1 Raw SiPM Signal processing

The raw signal that is produced by the SiPM is far too small to reliably measure with inexpensive equipment. This means that we have to amplify the signal first, before trying to measure it.

Low-noise signal amplification is an incredibly difficult job, which we are not nearly qualified for, in order to be comfortable designing our own circuit. Luckily, a lot of designs for various use cases are available on the internet. That is why we will not be designing this circuit ourselves, and we will

research usable circuits when we get to designing our own detector.

3.5.2 Electrical noise

Noise in the electrical signal can stem from multiple sources, some of them can be regulated, some of them cannot. The three primary contributors to noise are the power supply, noise stemming from the electrical grid, and noise that is generated by some electrical components in the circuits. [14]

The noise produced by the power supply can be minimised by choosing a quality power supply with low noise characteristics. The noise from the electrical grid and coming from other components, however, cannot be regulated.

This is where decoupling capacitors come into play. Noise caused by other circuit elements is shunted through the capacitor, reducing its effect on the rest of the circuit. Decoupling capacitors are typically placed at various sensitive parts of the circuit, with the other pad connected to ground. Different value capacitors are used to filter out different levels of noise. [14] (Appendix B)

3.6 Detector noise

A muon detector observes a quantum mechanical system, relativistic muons, and thus experiences a multitude of different statistical, quantum effects. Among these are “multiple scattering”, “energy loss” and detector timing intervals. These statistical effects cause a certain error in the measurements, causing measurements to not be completely accurate.

3.6.1 Multiple scattering

Multiple scattering is one of the biggest contributors to this inconsistency. This manifestation can be explained utilizing the physics behind materials. Scattering happens because small particles collide with the atoms in the material itself, this causes a deflection.

When this happens multiple times for a singular particle passing through a substance, it will produce a measurable difference in hit angle with the plane. This system can be visualized by the following schematic.

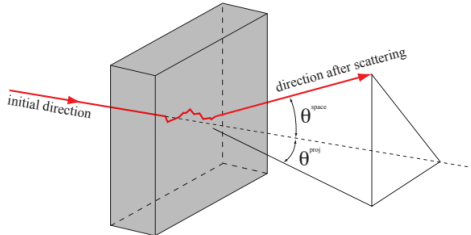


Figure 11: Schematic view of direction of a scattered particle. (Source: [15])

In this figure we see that a particle's trajectory is disturbed by the plate material causing an angular deflection, θ . This deflection can be quantized by the Highland formula (11).

$$\theta \approx \frac{13.6 \text{ MeV}}{\beta p} \sqrt{\frac{x}{x_0}} \left[1 + 0.038 \ln\left(\frac{x}{x_0}\right) \right] \quad (11)$$

This equation is experimentally defined—defined by observing experiments and formulating an equation which would explain these observations. If we simulate a situation using this equation, it produces a Gaussian curve as shown below.

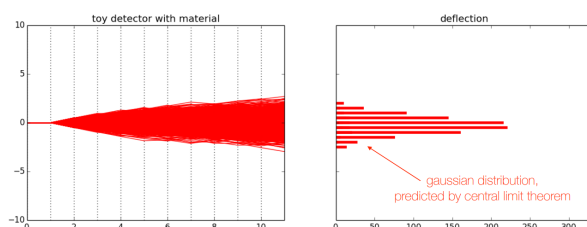


Figure 12: Figure illustrating Gaussian curve of the deflection using Geant 4. (Source: [15])

This figure shows that for the same muon in an equal system, the deflection can still differ. This is due to the fact that we are observing a statistical problem, in which statistics play an important role. This causes an eventual statistical error in reconstruction of hit and track values, because the muon or the emitted particle can be deflected changing its path.

3.6.2 Energy loss

When a muon passes through a material it loses energy due to a multitude of reasons. Among these are energy loss due to ionization and energy loss due to the effect of Bremsstrahlung. These effects are a lot smaller than the effect of multiple scattering, so the error they induce is also a lot smaller.

3.6.2.1 Loss due to ionization

When a muon passes through the plate, it excites the electrons in the material, causing it to go into a higher energy state which it later will “fall down” from, this is what produces the photon and is thus the reason we can measure the point of impact (POI) of the muon. This excitation and reaction costs energy though, for the muon. Resulting in a net loss of energy for the muon when it passes through the three plates. As a result of this energy loss, the characteristics of the muon change and thus the measurements change, causing a small error.

The amount of energy lost through ionization can be mathematically defined using an equation which describes the change in energy over a certain distance ($\frac{dE}{dx}$). This can be mathematically described using the Bethe-Bloch equation. The graph that represents this equation follows a Landau curve, a landau curve closely resembles a Gaussian curve and can thus be approximated as such. This is important, because the sum of the noise must be a Gaussian curve, in order to reliably do measurement.

3.6.2.2 Loss due to Bremsstrahlung

Bremsstrahlung, or braking radiation in English. Is a form of energy loss due to the acceleration of a charged particle, for both the positive and negative.

When a particle is decelerated it experiences a net loss of kinetic energy. This energy must go somewhere so it disperses as radiation, the

so-called Bremsstrahlung. Due to this loss of kinetic energy, the net energy changes of the particle.

In a detector this deceleration is caused by a muon being deflected by a nucleus or another electrically charged particle in the matter which it passes through. This deflection gives or takes energy, causing a change in velocity, which is what causes the Bremsstrahlung. The amount of energy lost over a certain distance can be defined by the following equation. [15]

$$(dE/dx)_{rad} = \frac{-E_i}{X_0} \quad (12)$$

This equation tells us, that the more energy a particle has, the more energy it will lose due to the Bremsstrahlung.

3.6.2.3 Total energy loss

The total energy loss for a muon follows a Landau curve as shown in the following figure.

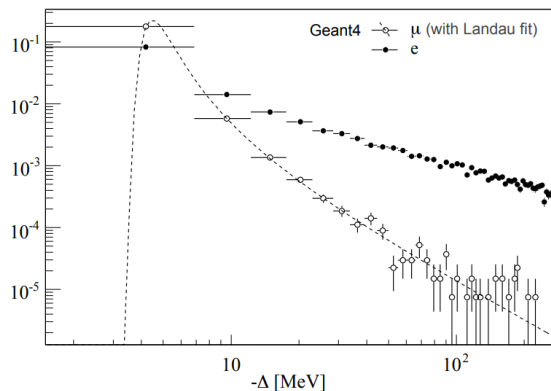


Figure 13: Loss of energy due to ionisation and Bremsstrahlung. (Source: [15])

This graph simulates a situation in which a muon and electron pass through a layer of material. All the variables are kept constant in this simulation. Yet we still see a Landau curve, so the same muon in an equal situation could experience a different energy loss. This is due to the quantum aspect of the problem. In the quantum world, almost everything is chance, nothing is certain. This shows that the error due to energy loss which Bremsstrahlung

causes, is not a fixed error, rather a Landau curve.

3.6.3 Error due to timing intervals

A detector has a certain time resolution; this is a certain value that describes the minimum interval between each measurement. This means that a certain measurement will always have a time inaccuracy, because in a set interval we are not exactly sure when a particle actually came into the detector. This error is a probabilistic phenomenon, and like many other probabilistic phenomena, it follows a Gaussian curve.

3.6.4 Theoretical resolution

The speed at which the photon moves through the scintillator medium is not the speed of light, because the light is not travelling in a vacuum. This alters the speed at which the photon travels, according to the refractive index (n) of the medium. The speed at which the photon moves through a medium, given its refractive index, is described by the equation below. This equation will later help us to determine how accurate our components should be to get a desired theoretical resolution.

$$v_\gamma = \frac{c}{n} \quad (14)$$

The refractive index varies significantly between scintillator materials. When looking at scintillator materials for muon detection and in particular, TOF-measurements, we see that EJ200 is one of the most popular scintillator materials for these use cases. [16] Luckily, both materials share the same refractive index, $n = 1.58$. [16] If we insert this value into (14), we get the following velocity of a photon through the scintillation medium.

$$v_\gamma = \frac{2.998 \cdot 10^8}{1.58} \approx 1.897 \cdot 10^8 \text{ m s}^{-1}$$

Using this velocity, we can create a rough idea of the timings required for a given resolution. Although this might seem a bit strange, we

will be rewriting this speed into a slightly strange unit, namely $ps\ mm^{-1}$. This is far from a standard unit, but it will give us a better idea of the planar resolution.

$$1.897 \cdot 10^8\ m\ s^{-1} \simeq 5.270\ ps\ mm^{-1}$$

Here, we can see that the photon's velocity equates to roughly 5 ps for every millimetre that it travels.

4 Detector design

Now that we have a fundamental understanding of cosmic ray muon detectors and the requirements needed, we can start engineering our own, optimal, cosmic ray muon spectrometer based on our set requirements.

4.1 System overview

The general idea of our detector is that we have a setup with two separate detector plates that are stacked perpendicular to each other. When a muon travels through the detector, we can measure two points of impact at separate heights. Given these two coordinates, we can reconstruct the vector of the original muon trajectory. Furthermore, we can potentially calculate even more advanced properties, such as energy and momentum

The plates consist of the required circuitry to calculate the original point of impact for the muon

4.1.1 Operating principles

When a muon passes through the plates of our detector, the ionization is triggered, thus producing a photon. Due to the wave properties of a photon, it will move radially outward [^2.4.1]. This wave will hit each corner of the plate at a specific time depending on the position of the initial impact, as the velocity of the wave is constant. Putting these readings together, we can calculate the original point of impact by performing a time of flight (TOF) calculation.

4.2 Detector assembly

The detector plates need to be oriented a certain way in order for the detector to function properly, the plates also need to be isolated from the environment. This is why it is important to create a proper assembly for the detector, which all starts with the plates themselves.

4.2.1 Detector plates

The heart of our detector is the detector plate, this is what is responsible for capturing the muon events and turning them into a signal that can be processed. As outlined in our design analysis, we will be making a scintillator-based detector plate [^3.3]. In order to be able to calculate the muon's trajectory—one of our design goals—we need to be able to measure the exact location of impact on the plate.

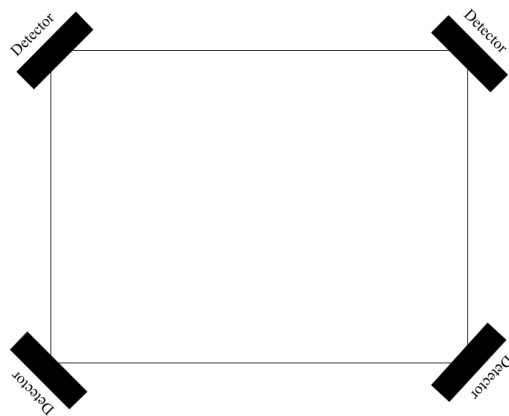


Figure 14: Schematic view of the construction of a single detector plate.

We do this by fitting a SiPM at each corner of the scintillator plate (Figure 14) and utilizing a TOF measurement, using the timing difference between SiPM's, to pinpoint the initial impact of the muon. This will give us 2-dimensional coordinates of the impact on both plates. If we then combine these two 2-dimensional vectors, along with their respective heights—based on the known distance between the detector plates—we can reconstruct a 3-dimensional vector, that describes the original trajectory of the muon.

4.2.1.1 Scintillator material selection

For our scintillator material, we have chosen to use BC-408. BC-408 is a plastic scintillator based on polyvinyltoluene that is extremely well suited for muon spectroscopy and TOF-measurements, while being more affordable than popular alternatives, such as EJ200. A list of the important parameters of the scintillator material is visible in the table below.

Parameter	Value
Refractive index (n)	1.58
Density	1.023 g cm^{-3}
Light output	64 %Anthracene
Ratio H:C atoms	1.100
Rise time	2.1 ns
Decay time	0.9 ns
Max emission wavelength	425 nm
Light attenuation length	210 cm

Table 1: Table listing the most important parameters of BC-408 scintillator material. (Source: [\[18\]](#))

As for the size of the plates, this is more of a trade-off between cost and event count, as larger detector plates, will allow more events to be captured. Looking at the standard cast sheet size for a 10 mm thick sheet, we see that the standard size is $63 \times 203 \text{ cm}$. [\[17\]](#) That is why we have decided to make the standard plate size $63 \times 63 \text{ cm}$, to maximise the available material. However, in the end it is still only a software defined value, so it could theoretically be any reasonable size.

4.2.1.2 SiPM-scintillator interface

Interfacing the SiPM to the scintillator plate is not as simple as putting the two next to each other. It is extremely important to properly couple them together using some sort of optical coupling compound—either a silicone pad or optical grease. This is done so that

there is no air gap between the scintillator and SiPM, which would cause a difference in the index of refraction, which in turn, would cause the photon to refract. Using the proper optical coupling compound—one where the refractive index is close to that of the scintillator plate and SiPM—would mitigate this.

Besides improving the refractive index, the optical coupling compound is also specifically designed to improve light transmission at the optimal wavelength. [\[19\]](#)

4.2.1.3 Optically isolating the scintillator plate

"Scintillation is an example of luminescence, where a scintillator material becomes luminescent when exposed to ionizing radiation, ..." [\[^2.4\]](#) Besides muon, there is also a lot of other ionizing radiation that just exists, not to mention that a SiPM detects photons, which means it would constantly detect every photon. This is why the plate construction needs to be properly sealed from external light and unwanted background radiation. As mentioned earlier, this is traditionally done using aluminium foil to block radiation and some sort of black vinyl—such as black electrical tape—to block out all remaining light. [\[^3.4.1\]](#) Doing this properly is essential for minimising background radiation pickup, which could disturb muon measurements.

4.2.2 Mainboard

Now that we can capture the muon events, we need a way to process and store them. Eight electrical pulses, coming from the two detector plates, need to be turned into usable data to be able to calculate the muon's properties, such as presence, trajectory, and velocity. Because the mainboard is a bit more complex than simply connecting some components together, we will be discussing it in more detail in the coming sections.

4.2.3 Housing construction

We have already discussed how the detector plates should be constructed [^4.1.1.3], but currently have no way of positioning these plates in such a way that would allow us to actually perform useful measurements. The calculation of the muon properties depend on the plates being perpendicular to, and at a known, fixed distance from each other.

The distance between these two plates does not matter that much, and should be configurable in software anyway, but for simplicity reasons, we have chosen to use a distance that is the same as the size of the plate, so that we get a cube detector. So the distance between the detector plates is, $h = 63 \text{ cm}$.

For the construction itself, we have decided to keep it relatively simple. The construction consists of a couple of pieces of aluminium extrusions that hold the two plates at a fixed distance, and gives a place to mount the mainboard. This will make it very easy to build the detector yourself as these materials are readily available.

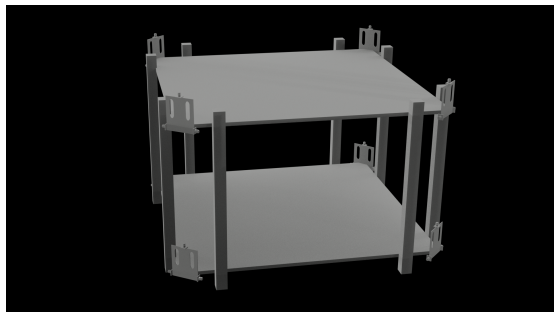


Figure 15: 3D-model of the general construction of our detector.

4.3 Electronic components

Now that we have a general understanding of the construction and the working principles of our detector, we need to choose what electrical components we are going to use. The most important components that need to be selected are the SiPM, the TDC

4.3.1 SiPM Selection

As a result of our selection process for the detection method of our detector, we have chosen to use a scintillator-based detector with SiPM sensors to detect the emitted photons [^3.3]. There are a lot of different types of SiPM's in varying price-ranges, as our goal is to build a relatively accessible detector, we have decided to use a readily-available and affordable sensor.

The most readily-available SiPM sensors are the Onsemi C-Series SiPM sensors, and it has actually been used by similar projects for the same purpose—muon detection—namely the Cosmic Watch and a research project by the University of Exeter. [20] (Appendix B & C)

The Onsemi SiPM sensor is one of the best sensors in the industry, while being available at a quite modest price. It is available in 3 different sensor sizes, with a subsequent 3 different microcell sizes. Listed below is a table comparing the different sensors, along with their respective prices.

Code	Sensor size	Microcell size	Price ¹
10010	$1 \times 1 \text{ mm}$	$10 \mu\text{m}$	N/A ²
10020		$20 \mu\text{m}$	€34,16
10035		$35 \mu\text{m}$	€16,94
30020	$3 \times 3 \text{ mm}$	$20 \mu\text{m}$	€16,95
30035		$35 \mu\text{m}$	€16,95
30050		$50 \mu\text{m}$	€16,94
60035	$6 \times 6 \text{ mm}$	$35 \mu\text{m}$	€23,09

Table 2: Table comparing the different versions of the Onsemi C-Series SiPM's. 1. The price listed for a single unit on Digikey as of 03-02-2026, 2. The MICROFC-10010-SMT has been discontinued, thus no price is available. (Based on: [20])

As for the size, while the price for the smaller sensor sizes may be cheaper, we have chosen to use the largest one; the 60035. This is because the larger size makes it much easier to work with, not only is it easier to solder, it

also leaves us with less tight tolerances when interfacing the sensor with the scintillator material.

In order to properly design the circuitry around this sensor, we need some basic information about the sensor. Luckily, Onsemi provides a very clear and detailed datasheet about the sensor series. The datasheet contains a table of performance parameters, these parameters indicate how the various versions operate and behave.

Besides the sensor and microcell size, some parameters also depend on the overvoltage. This is the difference in voltage provided above the breakdown voltage (V_{br}), which is typically $V_{br} = 24.5 \text{ V} \pm 0.2$. This overvoltage has an effect on the photon detection efficiency (PDE) and on dark current and dark count rate. [20]

The photon detection efficiency is relatively straight-forward, this tells us how efficient the detector is at detecting single photons, where a higher efficiency is better. Dark current is a little bit less trivial. Dark current is current that is generated by the detector, even when there are no photons detected. The dark count rate tells us how many of these events occur per second. In contrast to the PDE, these values should be minimised. However, it is worth noting that dark current can be filtered out by setting the correct threshold voltage for the detected value—which we will get into later—provided the dark current is lower than the normal current that occurs when a photon strikes the sensor. Below are two graphs comparing the effects of a given (over)voltage to the PDE and dark current. (Figure 16 & 17)

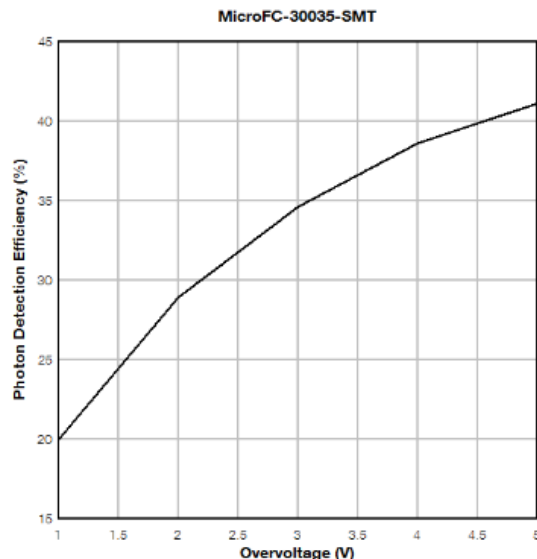


Figure 16: PDE at 420 nm versus overvoltage for the MICROFC-30035-SMT SiPM sensor. (Source: [20])

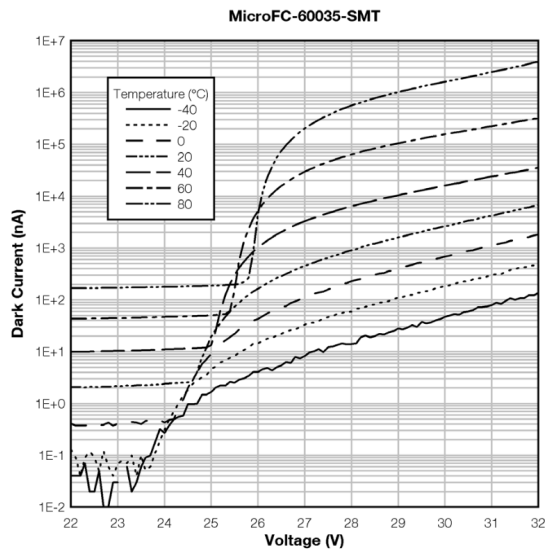


Figure 17: Dark current versus voltage and temperature for the MICROFC-60035-SMT. (Source: [20])

Having a look at the graphs, we can see that a higher overvoltage corresponds with a higher PDE and a higher dark current. As reflected by the Figure 17, the recommended overvoltage range is $V_{br} = [1, 5] \text{ V}$. This means that the supply voltage range should be $V_{supply} = [25.2, 29.7] \text{ V}$. If we take the maximum recommended overvoltage, the dark current is still manageable at only $0.6 \mu\text{A}$. The PDE however, is significantly higher

compared to a lower overvoltage, at 41%. (Figure 17)

Accounting for an overvoltage of + 5 V, listed below are the most important parameters for the SiPM sensor. (Table 2)

Parameter	Value
Breakdown voltage (V_{br})	$24.5 \text{ V} \pm 0.2$
Photon detection efficiency ¹ (PDE)	41%
Peak wavelength (λ_p)	420 nm
Gain	$3 \cdot 10^6$
Dark current (typical)	0.618 μA
Dark count rate (typical)	1200 kHz
Rise time	1.0 ns
Signal pulse width	3.2 ns
Temperature dependence of gain	- 0.8 %/ $^\circ\text{C}$

Table 3: Table listing the most important parameters of the MICROFC-60035-SMT SiPM sensor. 1. The PDE-value is measured at the peak wavelength. (Based on: [20])

4.3.2 Connecting the SiPM's to the mainboard

Our detector setup consists of two detector plates, with each four SiPM's, this means that we cannot directly connect each SiPM to the mainboard of our detector. Instead, we need to connect the SiPM's with cables. However, there are a few things that we should take into consideration when choosing what type of cables we are going to use, such as their resistance, attenuation—which is a direct consequence of the resistance, electromagnetic interference (EMI) and length.

The latter can be accounted for by using the same cable for each connection, this will ensure that the resistance and attenuation values will be the same, and we will thus not have any inconsistencies between sensors, which could interfere with the TOF measurements.

Luckily, there is a type of cable that is specifically designed for these types of application: coaxial antenna cable. Using SMA connectors—which are typical on coaxial cables—in combination with coaxial antenna cables, will minimise resistance, and thus the attenuation, and EMI.

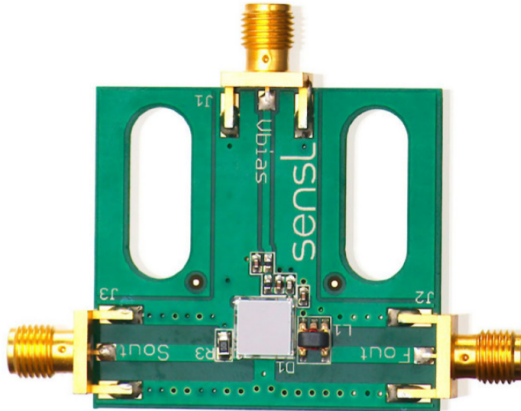


Figure 18: The MICROFC-SMA-60035 reference evaluation boards made for the 60035 SiPM sensor. (Source: [21])

Fortunately, Onsemi have released reference evaluation boards with SMA connectors which are quite suitable for our application. The boards feature a SiPM in the centre, with three SMA connectors for the bias voltage—the anode, the cathode and the fast output. [21] (Figure 18)

Using these boards will ensure that the connection between each sensor to the mainboard is identical, thus minimising difference between the sensors, and improving accuracy.

4.3.3 Timing equipment

As highlighted in our design analysis, we have chosen to use a timing system consisting of an FPGA. [^3.4.3] The primary requirement for the timing equipment is the timing accuracy, which we can calculate based on our desired planar resolution. As mentioned earlier, for a scintillator plate with a refractive index of $n = 1.58$ (Table 1), the resolution could be defined by the following value. [^3.6.4]

$$5.270 \text{ ps mm}^{-1}$$

This means that if we wanted to have a theoretical resolution of 1 mm , we would need a TDC that has a resolution of 5.270 ps or better. Since we wanted our detector to be able to measure trajectory quite precisely, while keeping cost manageable, we decided on a planar resolution of 1 cm . This means that the TDC's timing resolution should be at least 52.70 ps . To be on the safer side, we opted for a desired timing resolution of $30 - 45 \text{ ps}$, since there are always some discrepancies between the four SiPM's.

TDC timing resolution on FPGAs is determined by the carry chain delay—the propagation delay through each CARRY4 primitive in the FPGA fabric—which can be significantly different between different FPGA's.

Choosing the right FPGA that fits all our requirements, along with implementing time digital converters (TDC) with it, would take a lot of time as we would have to test a lot of different boards before coming to a conclusion, which would be beyond the scope of this project. That is why we have decided to look for examples where our required accuracy was reached with other FPGA's.

This led us to discover a research paper about a TDL-TDC implementation for FPGA's. The TDC was implemented on an AMD Artix™ 7 FPGA and has achieved single-shot precision of just 12 ps . This shows us that this precision is at least possible on relatively affordable FPGA's. [22]

After some more research, we discovered a project, where someone implemented a 4 channel TDC on the Digilent CMOD A7-35T. This was implemented using only consumer hardware and software, making it possible for us to replicate. The project used the Digilent CMOD A7-35T (XC7A35T) and achieved 35 ps timing accuracy, which would fit comfortably in our desired range. [23]

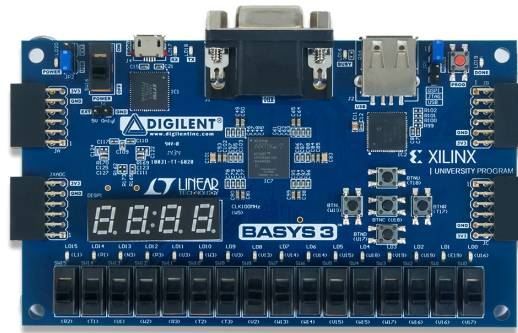


Figure 19: Basys 3 AMD Artix™ 7 FPGA Trainer Board (Source: [24])

After considering a couple of options, we have decided to use the Digilent Basys 3 featuring an AMD Artix™ 7 FPGA (XC7A35T). This is a relatively affordable FPGA board with features the same FPGA as the aforementioned project, while offering more expansion possibilities than the board they used. [24]

The FPGA also features enough resources to be capable of doing some real-time signal sanitization—filtering out false readings—and is capable of sending this data to an external pc, which can then further process this data to calculate the muon properties. This means, we do not need an additional microcontroller and can instead also use the FPGA for this.

Connecting peripherals to the device can be done by using either of the four Pmod12 connectors, these connectors feature two 3.3V, two GND and 8 GPIO pins. [24]

4.3.4 Signal amplification and capturing

As stated earlier, the signals originating from the SiPM are quite small and not reliably detectable by most microcontrollers. [^3.5.1]

We are, however, quite inexperienced in the field of signal amplification and will thus be borrowing a circuit from a different project.

After searching for designs that fit our requirements, we came across the amplifying, triggering and peak detection circuits of the

Cosmic Watch. This circuit has gone through a lot of iterations in order to work reliably. Coincidentally, the Cosmic Watch uses the same SiPM as we have decided to use, which means the design will work in our detector as well. A detailed analysis of these circuits can be found in Appendix B.

Besides amplification, the circuit also captures the peak of the SiPM signal, and keeps this signal high for a longer duration. This will make it a lot easier to trigger the microcontroller to fetch the amplified signal and reliably measure it. (Appendix B)

4.3.5 Signal measuring

Not all signals coming from the SiPM originate from muon detections. False readings can stem from multiple sources: background noise in the power supply or electrical grid, other components in the circuit, and dark current from the SiPM itself.

Most background noise stemming from electrical processes can be filtered out using decoupling capacitors, which we briefly discussed earlier. [^3.5.2] However, not all electrical noise can be filtered out, neither can the dark current from the SiPM. This is why it is important to also measure the height of the signal coming from the SiPM. This signal can then be compared to a threshold value, in order to determine if the signal comes from a muon impact.

However, the FPGA is not capable of reading analog values and will just interpret them as a digital value. This is where an analog to digital converter (ADC) comes into place. [^3.4.2] There are a few parameters that

determine an ADC's performance: resolution, channel count and sampling rate. The ADC for our detector must satisfy these requirements, which are the following: as mentioned earlier the resolution should be 12bit or higher [^3.4.2], the channel count should be at least 8, as our detector uses two plates with four SiPM's each. The sampling rate of the ADC is a little bit more complex, as the pulses are quite short. Luckily, our amplification and peak detector circuits captures the signal, and holds this signal high for a longer duration [^4.3.1.4]. This means that a sampling of 1 *MSPS*—which is quite common for low-cost ADC's—should be fine. 1 *MSPS* means that the ADC can perform one million samples per second, split across its channels if it is multiplexed or across all channels simultaneously if it is not multiplexed. So, if we choose an 8-channel, multiplexed ADC, that would yield us 125 *kSPS*, or 125 thousand samples per second per channel. This would mean that one cycle of sampling all 8 channels would take roughly 8 μs , which would give us plenty of time to process the data and re-prime the system for the next muon impact.

The ADS7028 fits the requirements exactly, it is an 8-channel, 12-bit, multiplexed ADC that has a sampling rate of 1 *MSPS*. It features a high-speed SPI interface and supports autonomous sequencing—scanning all channels in order, storing the results in a buffer and alerting the host about the results. [25]

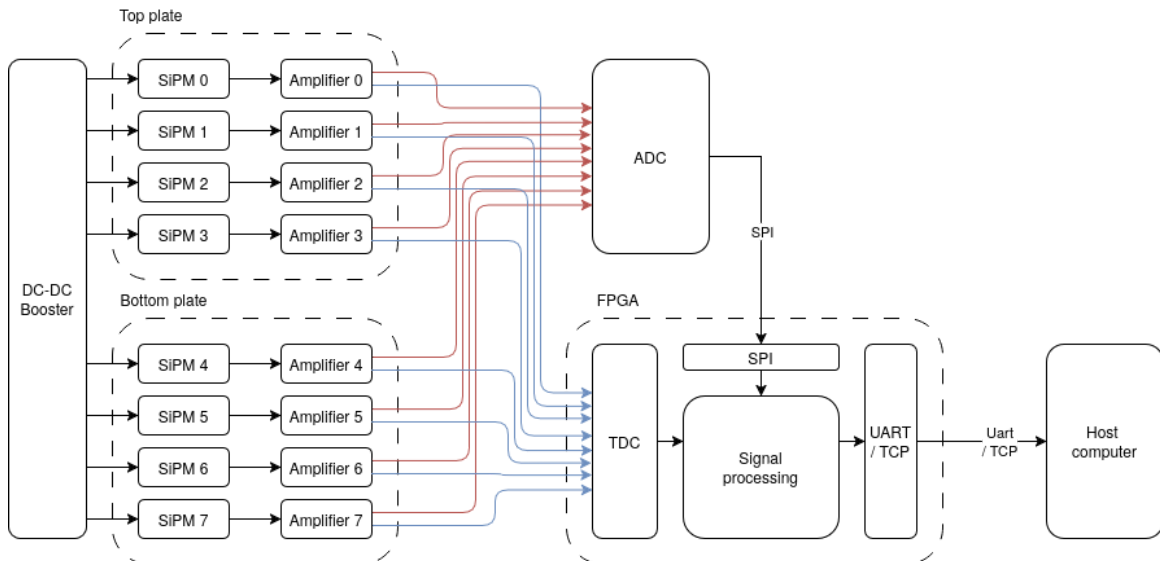


Figure 20: Diagram that visualizes the signal/data -flow that is required for the electrical circuitry.

4.4 Electrical circuitry

In order to simplify the circuit design process, we can visualize the required functions of our electrical circuit in a simple diagram, as can be seen in Figure 20. This diagram represents the working components of our detector, which will give us a rough idea what components interact with other components, and how they interact with each other. With this diagram, and with our prior research in mind, we can start designing the actual circuits.

The circuit starts with the DC-DC Booster, as a bias voltage of 30 V is required for the SiPM's. The output of each SiPM is connected to its own amplifier circuit, which ensures that the signal can actually be measured by our ADC. After that, a signal from each amplifier goes to our ADC, as well as the FPGA for the TDC measurement. Lastly, the data is sent from the FPGA to the host computer.

We will be designing all the components, except for the FPGA and host computer. All the separate components of the circuitry are explained below, and the entire schematic is present in Appendix D.

4.4.1 Design methodology

The schematics for our detector are designed in KiCad V9, which is an Open Source PCB design software, also called electronic design automation (EDA) software.

In the schematic we make extensive use of net labels, these are labels that can be placed in the schematic that act as a connection between said placed labels. This makes the schematic a lot clearer and makes it significantly easier to route. Keep this in mind when looking at the schematics below.

4.4.2 Power management

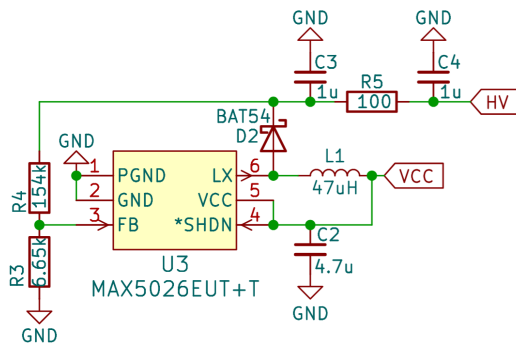


Figure 21: DC-DC Booster circuit of our detector.

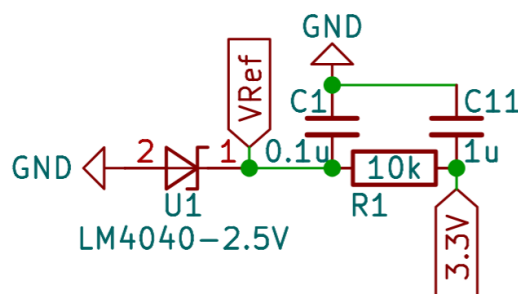


Figure 22: 2.5V Bias and reference circuit of our detector.

The power management circuits have largely been borrowed from the Cosmic Watch. (Appendix B) We have changed the component selection for some components slightly, but the overall working principles are exactly the same, a detailed analysis of their workings can be found in Appendix B. Our adaptations of these circuits can be seen in Figure 21 & 22.

4.4.3 ADC

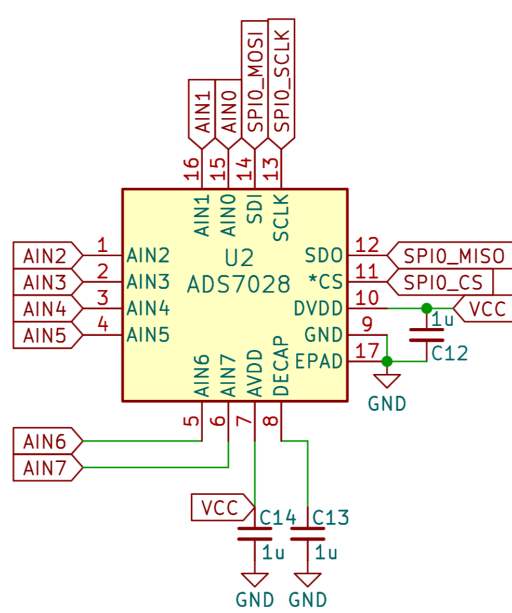


Figure 23: ADC circuit of our detector.

The ADC circuit [^4.3.5] is actually quite simple. The analog input pins, as well as the SPI pins, can be connected directly. The power pins, AVDD, DVDD and DECAP, do require some extra components, namely some decoupling capacitors. (Figure 23) Our design is based on the references and recommendations present in the ADS7028 datasheet. [25]

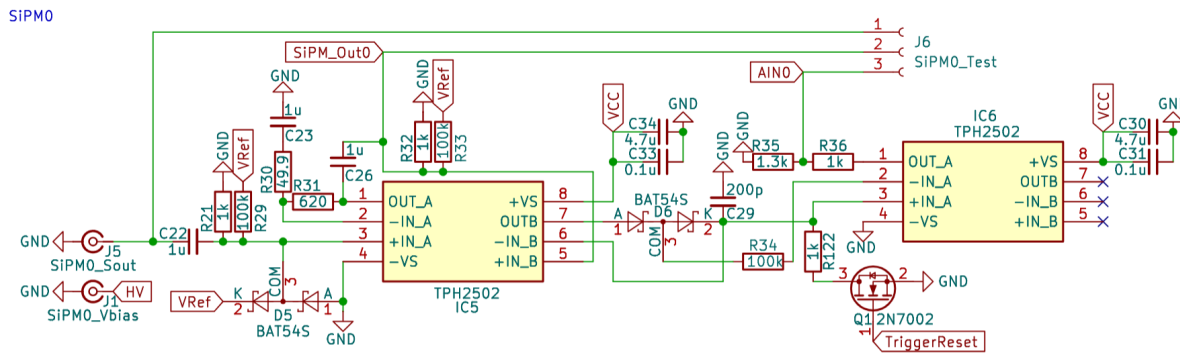


Figure 24: Amplifying and peak detecting circuits of our detector.

4.4.4 Amplifying and Peak Detecting circuits

This circuit is a bit more complicated, and has been changed quite a bit from the reference design. It is responsible for amplifying the raw SiPM signal and capturing its peak for easier ADC sampling. The entire amplification circuit can be seen in Figure 24.

If we start at the left, we can see two connectors, labelled *SiPM0_Vbias* and *SiPM0_Sout*. These connectors are the SMA connectors that connect to the corresponding connectors on the SiPM carrier boards. [^4.3.2] The first of the two, is connected to the DC-DC booster circuit using the *HV* label. The second connector is the output of the SiPM and feeds into the amplification circuit, as well as being connected to our first of three test points.

After that comes the first amplification stage, this boosts the raw SiPM to a much higher, readable voltage. Then it sends the signal to the TDC for the TOF measurement, it outputs to the second test point, and connects to the second amplification stage.

The second stage boosts the signal even higher, so that the ADC can more reliably read the voltage. The capacitor (*C29*) then captures the peak and holds the signal high for a much longer duration. This signal is then connected to the ADC (via *AIN0*), as well as the last test point.

The last part of this circuit is the resetting stage, this stage consists of a MOSFET that can be triggered by the *TriggerReset* line. When this line is pulled high, the MOSFET shorts the capturing capacitor (*C29*) to GND, thus draining it and resetting the system.

As labelled above, this circuit is for SiPM0, which means we need eight of these circuits in total, one for each SiPM.

4.4.5 FPGA Interface

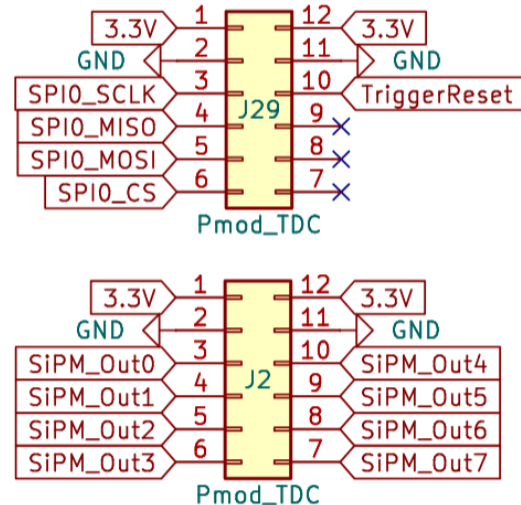


Figure 25: The two primary Pmod12 connectors for interfacing with the FPGA.

The last part of our circuit is the FPGA interfacing connectors, these connectors control all our circuits to the FPGA, so that it can actually perform the measurements.

It consists of two Pmod12 connectors—an open connector standard created by Digilent,

the manufacturer of our FPGA—which connect to two of the four Pmod connectors on our FPGA, leaving enough space for future additions. [24]

4.5 Data processing

Using the before mentioned electronic setup we attain the timing measurement of the photon hit on each of the SiPM's, using the difference in these values, we can calculate the point of impact (POI) and the trajectory using a TOF calculation. This is primarily done with help of χ^2 -minimisation.

4.5.1 Measuring muon impact

Given the aforementioned setup of the detector plates [^4.1.1], we get a certain time measurement t_i , for each detector i_n (with $n = 1, 2, 3, 4$). t_i can be theoretically expressed as the time when a muon hit the plane, plus the time it took the photon to travel the distance to the detector. We can mathematically express this using the standard formula for velocity (3) as the following:

$$\begin{aligned} t_i &= t_0 + t_{m \rightarrow i} \\ t_i &= t_0 + \frac{s_{m \rightarrow i}}{v_\gamma} \end{aligned} \quad (15)$$

With t_i being the time measurement from the detector, t_0 the time the muon hit the plane, $s_{m \rightarrow i}$ the distance from impact to the detector and v_γ is the speed of the photon. The speed of the photon is not the speed of light, because the light is not travelling in a vacuum, it's travelling through a medium, the scintillator material. This alters the speed at which the photon travels, according to (14).

$$v_\gamma = \frac{c}{n} \quad (^{14})$$

In this scenario, n is the degree at which a photon is slowed down by the material—the

refractive index. For our scintillator material, it is $n = 1.58$. (Table 1) [18]

We centre our plane, with the middle orientated on the origin of a graph (0,0). In this case, the detectors are orientated at

$(\pm L_x/2, \pm L_y/2)$ with L being the length of the plate in its respective direction (x or y) and in short the coordinate of a detector is $((x_i, y_i))$. The point of impact is (x_μ, y_μ) . Abstractly, this looks like the following.

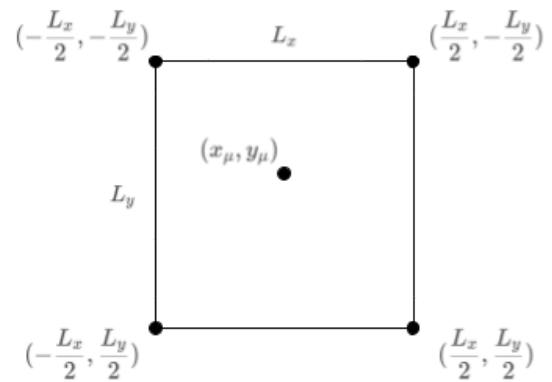


Figure 2: Schematic view of the coordinate plane.

In the aforementioned equation 1, the term $s_{m \rightarrow i}$ is not directly available. So we must derive it. This is easily done by the Pythagorean theorem. In our situation, this equation is mathematically defined as the following.

$$s_{m \rightarrow i} = \sqrt{(x_\mu - x_i)^2 + (y_\mu - y_i)^2} \quad (16)$$

If we substitute this into equation 1 we get the following equation.

$$t_i = t_0 + \frac{1}{v_\gamma} \sqrt{(x_\mu - x_i)^2 + (y_\mu - y_i)^2} \quad (17)$$

In this equation, t_0 remains undefined because we do not know the time at which the muon collided with the plane. This is not a problem because we have 4 of these time equations,

$i = 1 \dots 4$ and we have 3 unknowns, x_μ , y_μ , t_0 . So we can solve for all 3.

The most obvious and theoretical way to get these variables, is to just solve for x_μ , y_μ , t_0 .

But this approach relies on the fact that the 4 equations intersect at a singular point (x_μ , y_μ).

However, this is not the case due to noise in the readings, due to scattering, energy loss, detector inaccuracy and electronic jitter. This is why we use a method called χ^2 minimisation. [15] [26] [27]

What χ^2 -minimisation does is, it calculates a residual between a predicted and measured value and accounts for any predetermined inaccuracies of the detector, by dividing by the error in standard deviation form, σ . It calculates this value for multiple plates and adds this using a sum function. This way it reduces the error in the eventual measurement. Using an arg min function we can calculate a minimal value for χ^2 , this is the minimisation part, this minimal value is achieved when the predicted value is closest to the measured value.

As the predicted value we use equation 4, here are the 3 unknown parameters, x_μ , y_μ , t_0 . The arg min function calculates a minimum value for the residual, in order to achieve this minimal value it must attain the most accurate value for each of the parameters. These are the values for our point of impact, POI.

The σ in the χ^2 -minimisation calculations must follow a Gaussian curve, our errors are, or can be approximated as a Gaussian curve, making us able to use this form.

We can mathematically define the process as the following. The measurement residual can be defined as the following.

$$r_i(x_\mu, y_\mu, t_0) = t_{measured, i} - t_{predicted, i}(x_\mu, y_\mu, t_0) \quad (18)$$

This equation is written as a function of the parameters, we call these parameters in this case θ . So we get the following equation.

$$r_i(\theta) = t_{measured, i} - t_{predicted, i}(\theta) \quad (19)$$

We can substitute this into the χ^2 function.

$$\begin{aligned} \chi^2 &= \sum_i \frac{(Measured - predicted)^2}{\sigma^2} \\ \chi^2(\theta) &= \sum_i \frac{(r_i(\theta))^2}{\sigma_i^2} \end{aligned} \quad (20)$$

In this function i represents a non-defined amount of SiPM's. So when we do a measurement with 2 SiPM's we get the following equation.

$$\chi^2(\theta) = \frac{(r_1(\theta))^2}{\sigma_1^2} + \frac{(r_2(\theta))^2}{\sigma_2^2} \quad (21)$$

But we keep using the generalised function 6, this way we can do measurement with 3 or 4 SiPM hits, making the detector more efficient by not requiring all SiPM's to be hit and it makes it more generalised.

Now to finalise the mathematical foundation with the arg min function. With this we find the most optimal parameter measurement. This is mathematically defined as the following.

$$\theta_{best} = \arg \min \chi^2(\theta) \quad (22)$$

So the reason χ^2 -minimisation is so effective because it minimises the inherent error in measurement, because it uses the most measurements possible, and it produces a definitive value for the parameters, making the parameters easy to use in further calculations.

So after using χ^2 -minimisation for both plates, we get the following 2 values.

$$(x_{\mu}, y_{\mu}, t_0)_{Plate \ 1}$$

$$(x_{\mu}, y_{\mu}, t_0)_{Plate \ 2}$$

4.5.2 Reconstructing the muon's trajectory

Now that we have the coordinates for our muon. We have $(x_{\mu}, y_{\mu}, t_0)_i$, we also know

the z coordinate of the muon passing through each plate, because we know the distance with which we distanced the planes. So we define z_1 as 0 and z_2 as the distance between the plates. So mathematically, we can define this as.

$$(z_1, z_2) = (0, h)$$

This track can be defined by a vector, using multiple variables. Because there is not any real applied magnetic field, the trajectory would not be curved making it quite an easy, linear vector.

This linear vector can be defined by 3 parameters; it's (x, y, z) coordinates as a function of time. This results in a vector like the following.

$$\vec{r} = \begin{pmatrix} x(t) \\ y(t) \\ z(t) \end{pmatrix}$$

This vector tells us for each time measurement the corresponding (x, y, z) coordinate.

We can express $x(t)$, $y(t)$ and $z(t)$ as a starting position of the respective coordinate and the change in this position. For example, we can solve for the changing x using the derivative function of speed in the x direction;

$$v_x = \frac{dx}{dt} \quad (23')$$

$$dx = v_x dt \quad (23'')$$

If we now integrate both sides, we get a function of x with variable t . We get $v_x t$ and a constant, the constant equates to the starting position of x thus x_0 .

$$x(t) = x_0 + v_x t \quad (23)$$

This equation explains the x position with respect to time. We can use this same principle for the y and z direction so we get the following equations.

$$x(t) = x_0 + v_x t$$

$$y(t) = y_0 + v_y t$$

$$z(t) = z_0 + v_z t$$

In these scenarios, t is the time measurement, which we can approximate using the earlier found values for t_0 for both plates. Our detectors consist of two plates so we can generalize the values as $t_{0,i}$, where $i = 1, 2$ represent the separate detector plates. This value is the time when the light particle got emitted by the scintillator plate, thus the approximate time when the muon hit the plane.

We get the following vector when we substitute in our equations.

$$\vec{r} = \begin{pmatrix} x_0 + v_x t_{0,i} \\ y_0 + v_y t_{0,i} \\ z_0 + v_z t_{0,i} \end{pmatrix}$$

In this situation our unknown parameters are the following.

$$\theta = (x_0, y_0, z_0, v_x, v_y, v_z)$$

We can solve for these variables using χ^2 minimisation as well. In our scenario, our noise comes from the inaccuracy in the earlier

measurement; this error was due to the Gaussian noise of the aforementioned factors. So we can use the following, basic, equation for χ^2 minimisation.

$$\chi^2 = \sum_i \frac{(measured - predicted)^2}{\sigma^2} \quad (24)$$

With σ being the uncertainty in our measurement. In order to find our residual, we must look at the residual of each axis, x and y . For example, the residual for the x -axis would be the measured value minus the predicted value; the predicted value is the aforementioned equation for x . Mathematically, this looks like the following.

$$r_{x,i} = x_{measured,i} - (x_0 + v_x t_{0,i})$$

We can do the same thing for the z and y -axis.

$$r_{y,i} = y_{measured,i} - (y_0 + v_y t_{0,i})$$

$$r_{z,i} = z_{measured,i} - (z_0 + v_z t_{0,i})$$

The measured z is in this equation attained using the known height difference between the plates.

In these scenarios, i equates to the respective value corresponding to either of the 2 plates, so plate 1 or 2.

We can define noise in these 3 axes as well, so we get σ_x , σ_y and σ_z . We can now plug this into the χ^2 minimisation equation, we get the following.

$$\chi^2 = \sum_i \left(\left(\frac{r_{x,i}}{\sigma_x} \right)^2 + \left(\frac{r_{y,i}}{\sigma_y} \right)^2 + \left(\frac{r_{z,i}}{\sigma_z} \right)^2 \right) \quad (25)$$

Now, in order to get the right measurements for θ , we utilise the $\arg \min$ function again, and we get the following.

$$\theta_{best} = \arg \min (\chi^2)$$

$$\theta_{best} = \arg \min (\chi^2) \quad (26)$$

After we do this we get the right parameters for our vector and we thus have the correct vector corresponding to the trajectory of the muon.

4.6 Quantifying our detector

In order to correctly utilise the equations mentioned in the earlier chapters to calculate the muon's trajectory, we must know the error, also known as σ . We can obtain this error using Geant4 simulations.

Geant4 is a simulation toolkit written in C++, provided by CERN. [28] [29] [30] It simulates a beam of particles, in our case the cosmic ray, and it then simulates a detector measuring the particles. The amount of detected particles can then be used to calculate the error and efficiency of the detector.

In our previous calculations, 2 values for σ are used, the one in the hit reconstruction and the one in the track reconstruction. These 2 values are inherently different, yet they closely resemble each other. The only difference between the two is that in the σ for track reconstruction, the error due to multiple scattering between plates must also be added [^3.6.1]. We can express this as the following.

$$\sigma_{track} = \sqrt{\sigma_{hit}^2 + \sigma_{ms}^2} \quad (27)$$

The inaccuracy due to multiple scattering in our case is so negligible in comparison to the resolution of our detector, so we can approximate the σ_{track} as σ_{hit} .

So in order to find our accuracy for the detector we must use Geant4 to measure the "shot" particles against the detected particles of our detector.

4.6.1 Running the simulation

In order to properly simulate the cosmic ray hitting our detector and doing measurements on this, we must define a set of variables.

These variables fall under 3 “user initialization classes”:

G4VUserDetectorConstruction,

G4VUserPhysicsList and

G4VUserPrimaryGeneratorAction. In these classes we define the variables associated with their respective class.

For the detector construction, we define the world in which the reactions take place and what the geometry and materials are of our detector.

For the physicslist we define the physical processes which are simulated in our detector, things like Bremsstrahlung and multiple scattering.

For the primarygeneration, or “gun”, we define what particles are generated and “shot” at the detector. For us this is a cosmic ray.

4.6.2 Simulating the cosmic ray

In order to correctly simulate the cosmic ray, the *G4VUserPrimaryGeneratorAction*, we must define the cosmic rays properties. The properties we must define are the following: energy spectrum, angular distribution, charge ratio, spatial distribution and time structure.

We look at muons in our scenario, thus we only simulate the muons.

For the energy spectrum, a cosmic ray muon at sea level generally follows a spectrum like the following.

$$\frac{dN}{dE} \propto E^{-2.7} \quad (28)$$

This tells us that the amount of muons per energy “slice” are proportional to the energy to the power of -2.7. [31]

For the angular distribution of the cosmic ray muons. We use a formula for the intensity as a function of the zenith angle, θ . This function looks like the following. [32]

$$I(\theta) \propto \cos^2 \theta \quad (29)$$

This means that not all muons are shot straight from the z-axis onto the plane, but rather come from a lot of different angles.

The flux of our cosmic ray follows a regular amount of $1 \text{ muon cm}^{-3} \text{ minute}^{-1}$.

We must also define the charge ratio between the 2 types of muons, the positive and negative ones. These obey a charge ratio of around 1.2-1.3, so this looks like the following.

$$\frac{\mu^+}{\mu^-} \approx 1.2 - 1.3 \quad (30)$$

The muons also obey a spatial distribution, meaning they do not all get produced at the same x, y, z coordinates. To solve this problem we simulate the muons coming down from a plane above the detector, this plane is larger than the detector to simulate a realistic scenario.

4.6.3 Simulating the detector

We must also define the parameters of the detector itself, the *G4VUserDetectorConstruction*.

We place the detector in the middle of the created world volume, causing the simulation to run more symmetrically.

4.6.3.1 Simulating the electronics

Our SiPM detectors have an intrinsic noise due to electronic jitter and other quantum processes. This noise is incredibly hard to define in a simulation, so we use a process called smearing. Smearing “adds” a gaussian probability to our measurements after the initial simulation has been done, this acts and

uses the same values as the regular noise would, except it is way easier to define. There are three main variables contributing to the smearing effect, among these are PDE, gain fluctuation and timing resolution.

As aforementioned, see figure 17, the PDE of our SiPM detector is 41% and thus we use this value as the PDE value in the class for the smearing inaccuracy.

The gain in a detector can be primarily recognised as being proportional to the difference between the bias voltage and the breakdown voltage, thus it is proportional to the residual, the overvoltage. The primary contributor to a change in this gain, the gain fluctuation, is temperature. This changes the 2 voltage values causing an uncertainty in the overvoltage measurement and thus in the measured energy value.

In our SiPM the gain fluctuation due to the temperature variability is $-0.8\% /^{\circ}\text{C}$. This means that a 1 degree change in temperature from baseline, 21°C , results in a 0.8% change in voltage output. So a change to 22 degrees would result in a voltage measurement 0.8% lower than at 21 degrees for the same input energy.

The timing resolution of our system is defined by the timing resolution of the SiPM and the timing resolution of other electronics. The rise time of our SiPM is 300ps so this also becomes the timing resolution of our SiPM, because during the rise time, it is uncertain of the exact time thus it's representative of the timing resolution. The electronics used in amplifying and measuring the signal also add a certain time inaccuracy. The average uncertainty in time for the other electronics is 150ps. Both of these resolutions follow a Gaussian curve when measured. So in order to add the two we must square everything so we get the following timing resolution.

$$\sigma_{time, electronics} = \sqrt{300^2 + 150^2} = 335.4\text{ps}$$

We must also define the trigger threshold, which in our SiPM is around 10 PE, this means that it reads an impact when it measures 10 photoelectron hits. This is a regular value for cosmic ray detectors.

4.6.3.2 Simulating the scintillator planes

For the planes we use a scintillator material called polyvinyltoluene. For the simulation, we use the regular values mentioned by the facturer (*table 1*).

The density of the material is 1.023g/cm^3 and it has a refractive index of 1.58. The specific scintillator we use is the BC-408. This material has a H:C atom ratio of 1.104.

This scintillator material has a light output of 64% anthracene, this is approximately 10.000 photons per MeV. The rise time of the scintillator is 0.9ns and the decay time is 2.1ns. The peak emission wavelength of the scintillator material is 425nm. This value is only the peak, and for a simulation an emission spectrum is necessary, in order to make this a spectrum we approximate it as a gaussian distribution with a peak at 425nm. The width of the pulse is 2.5ns The light attenuation length is 210cm.

4.6.3.3 Simulating detector geometry

In order to run the simulation we define the geometry of the world in which we do the experiment as well. For this we must define the size of the world and what substance this world is made up of. Because we're simulating a cosmic ray in a non-vacuum scenario, we define the substance of the world as regular air so primarily nitrogen (78%) and oxygen (21%). Our detector must fit in the world in which we place it, we must also make sure the simulation happens according to a real life scenario. This is why we use quite a large simulation world of $500\text{cm} \times 500\text{cm} \times 500\text{cm}$ in the respective x, y, z dimensions.

In this world we position our detector in the center of the 3 dimensional system. So the center of mass of the detector is placed at $x = 0, y = 0, z = 0$. The scintillator planes are each 63cm by 63 cm and are 10 mm thick. The planes are each separated by 63cm. This means that the center of the first plane is located at (0, 0, 0), for the second detector this is (0, 0, 63) in their respective directions.

Our SiPM's are set up at each corner of the planes to measure the photons. So in total 8 SiPM's. These SiPM's are the parts actually doing the measurement. These SiPM's each have a sensor size of 6mm and a microcell size of 35μ . In our simulation, these SiPM's are optically coupled with EJ-550, which has a refractive index of 1.48.

4.6.4 Defining the physical processes

The physical processes must also be added to the simulation. These processes will then be used in the calculations and measurements in the geant4 application.

In our simulation, multiple scattering, Bremsstrahlung and energy loss are the most important physical processes. Also the regular physical processes like decay, ionic physics and hadronic physics. And thus these are used. Also in order to run the simulation we must import photon processes, because we're working with a scintillator based detector.

4.6.5 Executing the simulation

In order to run the simulation we must specify the amount of particles the cosmic ray shoots. For this value we use 10.000, because a too large amount would cause the user's computer to overload, causing the simulation to crash. 10.000 simulated particles will give us an accurate measurement, yet still retain the ability to be run by an average computer.

Once the simulation is run using CMake and visual studio, we get a root file. We analyse this file using Python, producing the plots and data which we can use. Among these plots are

hit-plots, angular distributions, energy and angle efficiency, hit residuals, efficiency and SiPM performance.

4.6.6 Results

When the simulation was run we got the following results.

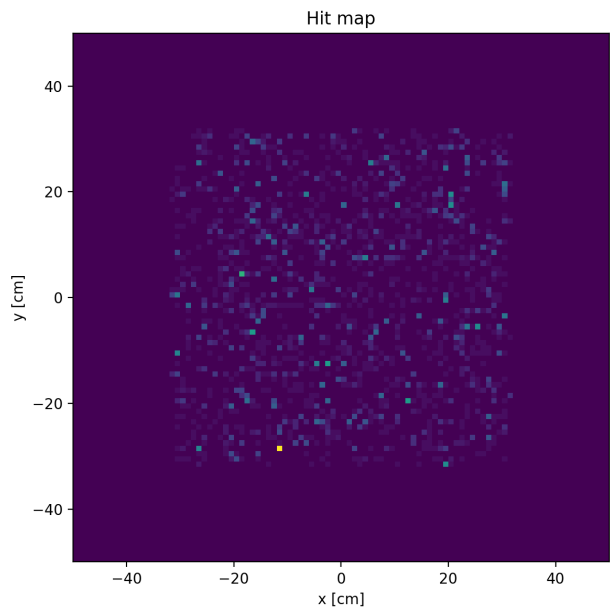


Figure ...: Simulated hitmap on a resulting from the Geant4 simulation.

The hitmap plot shows the area and places where a muon hit was measured. A blue/orange color indicates a muon hit, with a more vibrant color being more hits. The reason the activity measured on the edges is 0, is because the detector only detects a particle when it passes through both planes. Our planes are 63cm x 63cm, so on the edge of this plot ($x > \frac{63}{2}$ or $y > \frac{63}{2}$) fall outside the range of the first or second detector due to the angular distribution, thus are not measured. The random results in this graph are as expected, because a cosmic ray does not have a "preference" of origin. The angular distribution is shown in the next graph.

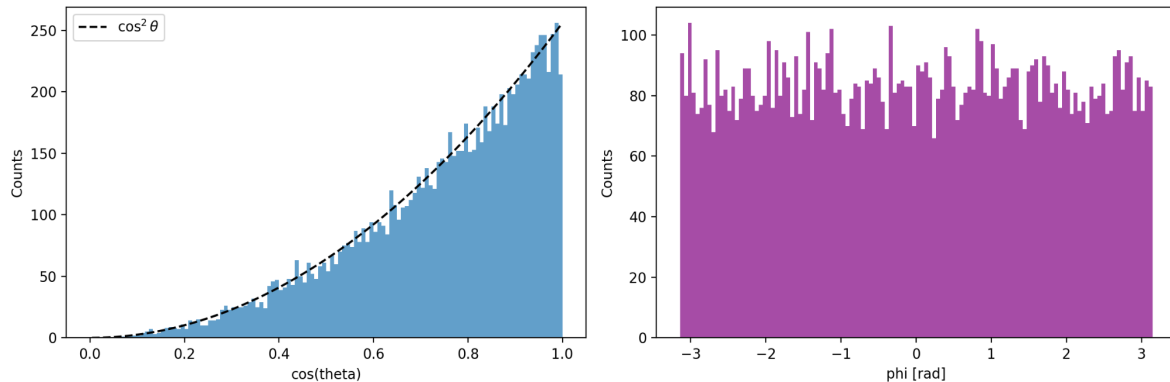


Figure ...: Simulated angular distributions of the cosmic ray.

In the left graph we see a regular $\cos^2 \theta$ curve plotted next to our $\cos(\theta)$ results. These lines follow the same fit, this means that Geant4 correctly simulated the $\cos(\theta)$ distribution. The graph has some inconsistencies, these are due to the error in measurement and due to statistics, because we only simulated 10.000 muons. In the right graph we see the azimuth angle. This angle can be fitted as a straight line, this is normal for a cosmic ray, because the ray is isotropic and thus produces the same amount of particles from the North, East, South and West directions.

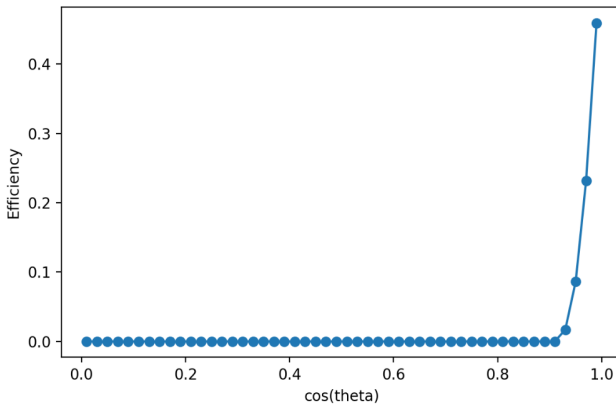


Figure ...: Simulated efficiency in measuring a muon from different angles.

The graph above shows the angles at which our detector effectively measures the particle. The efficiency is defined by the amount of

measured muons divided by the total amount of produced particles. This efficiency rises with a higher $\cos(\theta)$ angle. This makes sense because in order for a particle to be detected, it must pass through both planes and thus correlates with expectation. The chance for a particle to pass through both planes is higher when it passes straight down. So at a smaller angle (so a higher $\cos(\theta)$ value), the efficiency will be higher. The overall efficiency is shown in the following graph.

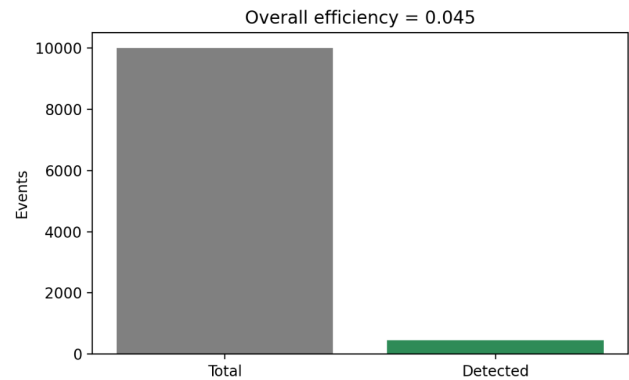


Figure ...: Simulated total efficiency.

This figure shows that of the total 10.000 simulated events a mere 449 were measured by the detector. These 449 are the events which triggered a response in both planes. The reason for this is that a hit only gets registered when a large number of prerequisites are met. Among these are that it must be measured by

3 or more SiPM's, the signal must have a certain strength, which is 10 PE. These prerequisites make it so the bad measurements are filtered out, so we get measurements with less noise. The negative thing is that we lose a large amount of measurements. This value was as expected due to the extensive requirements set on the hit registration.

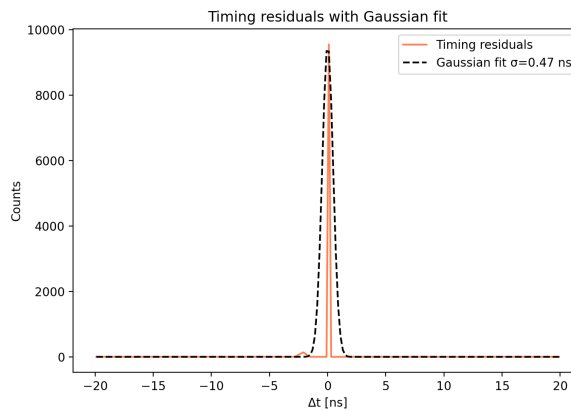


Figure ...: Simulated residual of timing measurements.

This graph shows the timing difference between the 2 plates. This follows a Gaussian curve with the σ being 470ps. This timing difference is calculated by subtracting a predicted value for Δt by the measured Δt data. The residual is generally at 0, showing no systemic bias in the timing measurement between the 2 plates. This is because in most cases $\Delta t_{predicted} = \Delta t_{measured}$.

The $\Delta t_{predicted}$ in this case would be the speed of the muon, which is really close to the speed of light so $0.99c$ divided by the distance between the 2 plates so 0.63m. When we do this calculation we get the following.

$$\frac{0.63}{0.99c} = 2123\text{ps}$$

The sigma of 470 ps shows the total timing resolution between the 2 plates. Thus, the relative uncertainty between the 2 plates would be the following.

$$\frac{470}{2123} \times 100\% = 21\%$$

The spread comes from the inaccuracy in timing measurements on single planes. Thus creating a Gaussian curve. Following this measurement we can also calculate the single plate timing resolution. When we assume both plates have the same intrinsic error in timing measurement we use the following formula to calculate the single plate timing error.

$$\sigma_{single\ plate} = \frac{\sigma_{total}}{\sqrt{2}}$$

$$\sigma_{single\ plate} = \frac{470}{\sqrt{2}} = 335\text{ps}$$

This is the same approximated value as mentioned previously in chapter 4.6.3

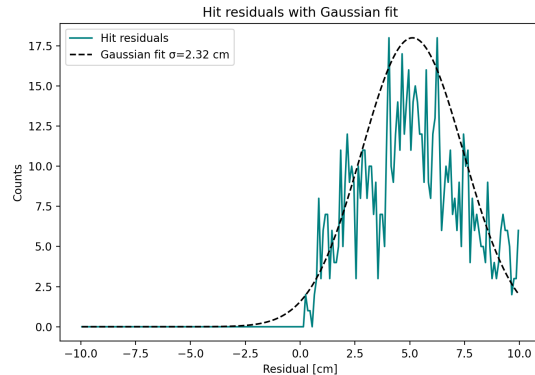


Figure ...: Simulated residual.

The figure above shows the simulated error in the hit measurement on a single plane. It shows a Gaussian curve with the σ being 2.32 cm. This means the detector hits are accurate with an error of 2.32 cm. This is also the sigma used in the χ^2 -minimisation.

This value for sigma is enough for educational level track and hit reconstruction. The track is quite accurate, this means that other measurements like momentum will also be quite accurate, especially for an educational environment.

4.7 Calculating the properties of the muon

Now that we have all the necessary data and parameters, we can use these to calculate the properties of the muon, such as its velocity, momentum and energy.

We are dealing with relativistic muons, we must thus obey the rules of relativity as mentioned before. Quite a large portion of mathematics in relativity is based on the Lorentzfactor.

In order to calculate the Lorentzfactor for the measured muon, we must first find the velocity of the muon. We can start finding the velocity by creating a vector for the velocity. This vector is comprised by the earlier attained speed in a separate x , y , z direction from χ^2 minimisation. Such a vector would look like the following.

$$\vec{v} = \begin{pmatrix} v_x \\ v_y \\ v_z \end{pmatrix}$$

Now that we have the speed vector we can calculate the actual speed by using the Pythagorean theorem, this results in the following equation.

$$v = |\vec{v}| = \sqrt{v_x^2 + v_y^2 + v_z^2}$$

Now we have the speed of the muon and can thus calculate the Lorentzfactor for our measurements, which would equate to the following.

$$\gamma = \frac{1}{\sqrt{1 - (\frac{v}{c})^2}}$$

In order to calculate the momentum of our muon we use the relative function for momentum which is the following.

$$p = \gamma mv$$

For the total energy of the muon we use Einstein's famous equation $E = mc^2$ for relativistic scenarios, so the following.

$$E = \gamma mc^2$$

4.8 User interface

Now that we have attained our data we can start visually showing the items found. We do this using easily accessible software.

Our main goal for our project is to introduce particles and particle spectroscopy in an accessible but extraordinary manner. We want to make sure the software follows these primary rules.

The detector attains the trajectory vector. In order to visually show this data, we use a 3d graph to illustrate the actual movement of the particle, to make it even more extraordinary. This looks like the following figure.

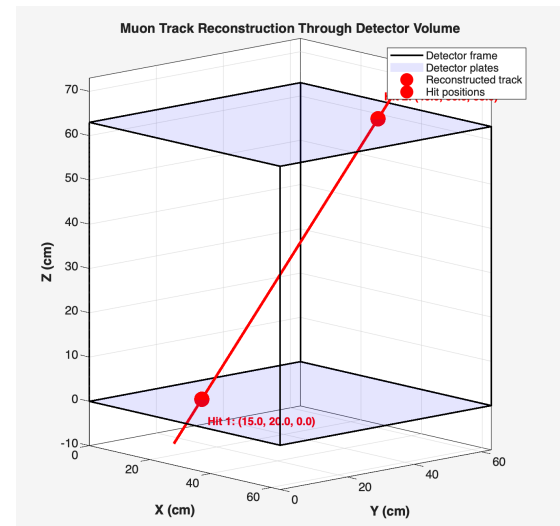


Figure 14: Visualization of the muon trajectory.

We also attain physical measurements, like velocity. We show these measurements on a graph and in pure data, a root file, which is able to be exported by the user. This gives the user the ability to analyse the data for themselves, or just demonstrate the measurements directly.

In order to make the software accessible, it must utilize an easy-to-use interface. No excessive code, just concise parameters. We show the raw data using tables and graphs.

The user clicks on a button to start the measurement software. Then the values get shown in the tables and the graphs. The user can cycle through different measurements and reconstructed track data.

4.9 Cost estimates

Estimating the cost of the detector is a bit tricky. The total cost for all the components that populate the PCB is €62.36, as is outlined by the BOM in Appendix E. However all the other components, namely the SiPM boards, scintillator plates, SMA cables, construction and housing components and the cost of the PCB itself are a bit trickier to calculate.

The SiPM boards are available on Digikey for around €290 per piece, however we assume that you can get them for cheaper from Onsemi themselves, but generally we think that these boards would total around €2000 when purchased in batch.

Getting $63 \times 63\text{ cm}$ BC408 scintillator plates requires us to get a quote from the manufacturer, however we did not get a response from Luxium—the manufacturer for BC408 scintillator plates. However, when looking at smaller plates of the same material we estimate a plate of this size would roughly cost around €2000 as well.

All the other components, such as the SMA cables, housing and PCB are quite a bit cheaper and those components would total around €500 if we were to give a rough estimate.

In total, that would land us at around €5000 for material costs, although this can be quite high for some students, it is still cheap compared to consumer and more high-end solutions.

III

The end of a chapter

5 Conclusion

Our goal in this paper was to construct a cosmic ray muon detector which shows interesting and precise, quantitative measurements, and yet is still affordable and usable in educational environments. By researching what precisely a muon detector is, what components are needed to perform muon detection, and how to use these components properly, we have achieved our goal.

5.1 Our approach

We approached the issue by using a scintillator-based detector. Our design consists of two $63\text{cm} \times 63\text{cm}$ BC-408 scintillator plates placed 63 cm apart from each other. Both scintillator plates are equipped with 4 Onsemi MICROFC-60035-SMT SiPM sensors. When a muon travels through the scintillator, it excites the electrons in near atoms, causing these electrons to reach a higher energy state and later falling back down, releasing a photon. This photon radiates outward, and can thus be measured by the SiPM's at each corner of the plate.

Due to a difference in time measurements, we can triangulate the signal, resulting in a position measurement. In order to triangulate these signals we use χ^2 -minimisation, this is necessary due to the statistical uncertainties in the measurements. Using the time and hit measurements of the muon, we can calculate advanced muon properties, such as the original trajectory, momentum and energy of the muon.

5.2 Findings

In order to get a better understanding of the performance of our detector, we have simulated it using Geant4—a simulation toolkit created by CERN, that is used to simulate the passage of radiation through matter—this simulation yielded the following performance parameters. (Table 3)

Parameter	Value
Total event	10000
Detected events	449
Overall efficiency (%)	4.5%
Track residual σ	2.32 cm
Hit residual σ	2.32 cm
Timing residual between plates	0.473 ns

Table 3: The performance parameters that were yielded by our Geant4 simulation.

These results have shown us that our detector has detected 449 muons for the 10000 total events that it was simulated with. This results in an effective efficiency of 4.5%. This value might seem low, but the reason for this is that we prioritise an accurate measurement over a high quantity of measurements. Our hit measurements are accurate with an error of 2.32 cm on each hit, this means that the measurement is reasonably accurate for a low-budget muon spectrometer. The timing residual between the two used plates is 0.473ns which strongly resembles a theoretical, real-time measurement. This shows that the detector is theoretically accurate and should be able to accurately measure data in a real situation.

5.3 Significance

Even though it was not possible to fully build the detector and test it, we created a good foundation for other projects to build upon. This makes the possibility of creating an accessible scientific-grade muon detector that is capable of calculating advanced muon properties more feasible and can kickstart other projects. This gives students and low-budget research facilities a way of learning the beauty of particle physics and cosmic behaviour, and potentially provide a good basis which they can base their own, even more advanced detector upon.

6 Discussion

The findings presented in chapter 4 & 5 showed that the detector we engineered theoretically works and that it has an accuracy of 2.32cm and an efficiency of 4.5%. We attain these values with a detector with a size of $63 \times 63 \times 63\text{ cm}$ and it is also relatively affordable, in comparison to high-end detectors, at around €5000 as of the time of writing this paper. [\[^4.9\]](#)

6.1 Interpretation of results

The simulation using Geant4 shows us important characteristics of our detector. Firstly, the spatial resolution of 2.32cm represents the inherent inaccuracies when working on a quantum scale. Yet for educational purposes it still suffices.

Secondly, the timing resolution between the 2 plates of 470ps represents a relative 21% timing resolution between the plates. This allows for reasonably accurate velocity measurements, especially for an educational environment. This timing resolution also reveals that our detector should be able to distinguish between muon events, when utilised with the same hit requirements (strength, amount of SiPM's etc.) as used in the Geant4 simulation.

The spatial resolution of 2.32cm allows for relatively accurate track reconstructions, which help in increasing the educational value.

Although the efficiency of 4.5% looks small, it is perfectly reasonable. Utilising the average cosmic ray muon flux of $100\text{ m}^{-2}\text{s}^{-1}$ mentioned in paragraph 2.1.1 and our detector being $0.63^2 \approx 0.40\text{m}^2$ the amount of incidents per second would be around 40. With an efficiency of 4.5%, we would get approximately 1.8 muon hits per second, or expressed in minutes; 108 muon hits per

minute. This is more than sufficient for a physics demonstration.

The lower efficiency is a deliberate choice which we made—we want to prioritise accuracy over quantity, and since decreasing the hit requirements would significantly decrease the accuracy—we chose to stay with the lower efficiency.

6.2 Design goals

In chapter 3 we created a set of goals which we wanted to achieve when engineering the spectrometer, among these are design requirements and technical requirements.

The goal was to create a cosmic ray muon detector which shines a new light on teaching particle physics and high energy physics and yet is still affordable for an institution and is able to be put together by the institute. We achieved this by creating the framework for a scintillator-based SiPM spectrometer. The detector calculates the hit position and time data of a muon hit on 2 plates and then we provide a foundation on how to actually do measurement and calculate trajectories using this hit data. The detector does this without costing a fortune like high tech CERN pixel detectors.

Due to the fact that we attain a trajectory of the incoming muon, we can visibly show this in a graph, and do calculation using the trajectory vector. This gives the user an actual view of how the muon moves in real-time, instead of a mere mathematical description of how a muon works. Thus achieving the first goal of engineering a detector which makes particle physics more enjoyable.

6.3 Limitations

The project was not exactly an easy feat to tackle, so there were times in the project's span when we had trouble with our knowledge or were limited by either time or materials.

Perhaps the biggest roadblock we hit was the lack of time that was left to create the firmware for the detector and the accompanying software which is able to be used with our detector. This is also our biggest point of regret, given that the software is what ties the whole product together and would have made it a lot easier to view the project as a whole. Nevertheless, we did provide the mathematical foundation and formulated our goals and requirements for the software, so there is definitely enough room for further research on this topic.

Midway through the project, when researching existing projects we came up with the idea to actually build the Cosmic Watch itself, to get an even better understanding on how it works, and to have even more knowledge to base our design on. However, we have not been able to finish the detector before the deadline of our project, because of a lack of time and an issue with the material sourcing. Despite this, we still managed to make a detailed analysis of the Cosmic Watch, which we have used extensively in the research stage of our project. (Appendix B)

The last limitation is the lack of evidence that our detector actually works. Although we have proven that it could theoretically measure the muons and calculate useful data with the Geant4 simulation, we have no way of knowing if the detector would actually function in the real world, as we have not validated our circuit designs and actually built and tested the detector.

6.4 Further research

Due to the limitations of the project, there is plenty of room for improvement upon the current design.

Firstly, it is necessary to build and code an accompanying software for the detector, which calculates the tracks and other variables. The software must also include the visualisation like the trajectory reconstruction

images and tables. It is also required to calibrate the used electronics in this software.

Secondly, there is still room for improvement in the accuracy and efficiency of the detector. Even though the detector is theoretically viable, with more knowledge and investments there are still upgrades to be made in terms of timing and spatial resolution.

Thirdly, the detector itself must also be built. This can be a challenge to conquer. To physically build the muon spectrometer and test it in real-life scenarios, instead of with a virtual simulation.

Lastly, the price of the spectrometer is still reasonably high, this is primarily due to the expensive scintillator materials used. To battle this, future research can focus on providing new ways and materials which have scintillator properties, causing the detector to be more affordable for the educational institutions.

6.5 Comparison

A lot of components of the detector are based upon the Cosmic Watch, which also shows in the schematics, as they are quite similar to theirs. Despite this, our detector is still quite a bit different from the Cosmic Watch in terms of capabilities, where it would actually be closer compared to the research project by the University of Exeter. (Appendix C) So, our detector is more of a mix between all the existing projects that were discussed throughout our paper.

6.6 Applications

In the introduction we mentioned the implications which our project provides. Using this blueprint of the spectrometer, a user will be able to reliably measure and show the beauty of physics to an audience whom does not necessarily understand the entire mathematical foundation, which makes it hard to initially visualize a muon. Using our device,

the user is able to view the trajectory of the muon and calculate properties of this muon, which also make it educational. Another application is that the measuring properties of the eventual spectrometer can be used by another group for their final research project for high school students. This way we can further increase our knowledge and interest into the beautiful field of physics.

6.7 Reflection

Physics is an incredibly in-depth field of work, the more you think you know about the field, the more you realise how little you actually know. This brings challenges, however this is the precise beauty of this sector.

One of the biggest challenges we faced during the project was understanding how to measure something so small like a muon on a scale of that of humans. Eventually we conquered this challenge with a lot of work and dedication and eventually found and understood the scintillator based muon spectrometer using a silicon photomultiplier.

Another big challenge was to actually measure the signal provided by the SiPM's, as these signals are extremely small and difficult to measure reliably. Because of this, we needed to implement an amplification stage, however, high speed signal amplification is an incredibly difficult job and could have been a separate paper by itself. Even though we have borrowed most of the amplification circuitry from another project, it was still a challenge to incorporate it in our project

The last and final challenge was to realise a mathematical foundation for reconstructing hit and tracks. This was incredibly difficult due to the statistical properties of particle physics. We eventually found the algorithm called χ^2 -minimisation.

The difficult aspects of this paper are exactly what makes the final product even more rewarding.

References

1. Bouwens, R. E. A., Kranendonk, W., Van Lune, J. P., Prop - van Den Berg, C. M., Van Riswick, J. A. M. H., & Westra, J. J. (2022). *Binas: Informatieboek havo / vwo voor het onderwijs in de natuurwetenschappen* (7de editie). Noordhoff Uitgevers.
2. L'Annunziata, M. F. (2022). *Radioactivity: History, Science, Vital Uses and Ominous Peril*. Elsevier.
3. Jacques Marteau, Jean de Bremond d'Ars, B. Carlus, A. Chevalier, A. Cohu, et al.. Development of Scintillator-Based Muon Detectors for Muography. L.Oláh; H.K.M. Tanaka; D.Varga. *Muography: Exploring Earth's Subsurface with Elementary Particles*, 270, American Geophysical Union - Wiley, Chapter 17 237-252, 2022, Geophysical Monograph Series, 9781119723028; 9781119722748. [⟨10.1002/9781119722748.ch17⟩](https://doi.org/10.1002/9781119722748.ch17). [⟨insu-03575649⟩](https://doi.org/10.1002/9781119722748.ch17)
4. Wikipedia contributors. (2026, Februari 11). *Wave-particle duality*. Wikipedia. https://en.wikipedia.org/wiki/Wave-particle_duality
5. Bangaru, N. (2024). *Design and Testing of Gaseous Detectors and Their Readout Electronics for Particle Detection at High Counting Rates*.
6. Wikipedia contributors. (2025, November 22). *Wire chamber*. Wikipedia. https://en.wikipedia.org/wiki/Wire_chamber
7. cell.png. (n.d.). <https://cds.cern.ch/record/2705998/files/cell.png>
8. Wikipedia contributors. (2026, Februari 11). *Photomultiplier tube*. Wikipedia. https://en.wikipedia.org/wiki/Photomultiplier_tube
9. *What is an SiPM and how does it work?* (2016, October 7). Hamamatsu Photonics. <https://hub.hamamatsu.com/us/en/technical-notes/mppc-SiPM's/what-is-an-SiPM-and-how-does-it-work.html>
10. Haddad, Y. (2020). *Upgrade of the CSC Muon System for the CMS Detector at the HL-LHC*. 837. <https://doi.org/10.22323/1.398.0837>
11. Resnick, B. (2019, July 25). *Extremely powerful cosmic rays are raining down on us. No one knows where they come from*. Vox. <https://www.vox.com/the-highlight/2019/7/16/17690740/cosmic-rays-universe-theory-science>
12. *ADC*. (n.d.). Analog Devices. <https://www.analog.com/en/resources/glossary/adc.html>
13. Schneider, J., & Smalley, I. (2025, November 17). *Field programmable gate array*. IBM. <https://www.ibm.com/think/topics/field-programmable-gate-arrays>
14. Noise generation Sources & reduction Techniques. (n.d.). RF Wireless World. <https://www.rfwireless-world.com/articles/noise-generation-sources-reduction-techniques>
15. A. Salzburger. (2018, January 4). *Track Reconstruction in High Energy Physics & in the era of Machine Learning/Data Science* [Slide show]. Spatind Conference. CERN. <https://indico.cern.ch/event/666278/contributions/2830627/attachments/1579364/2495228/2018-01-04-Salzburger-Spatind-Conference.pdf>

16. Copeto, P. (2023). *Muon detection with a scintillator-PMT based setup*. LIP. <https://www.lip.pt/files/training/papers/2023/pdf/2023-PAPER-154-4.pdf>
17. BC400, BC404, BC408, BC412, BC416. (n.d.). Luxium Solutions. <https://luxiumsolutions.com/radiation-detection-scintillators/plastic-scintillators/bc400-bc404-bc408-bc412-bc416>
18. BC-400,BC-404,BC-408,BC-412,BC-416 Premium Plastic Scintillators. (2023). Luxium Solutions. https://luxiumsolutions.com/sites/default/files/2023-08/146337_Luxium_SGC%20BC400%20404%20408%20412%20416_FIN.pdf
19. Assembly materials. (n.d.). Luxium Solutions. <https://luxiumsolutions.com/radiation-detection-scintillators/assembly-materials>
20. C-Series SiPM Sensors: Silicon Photomultipliers (SiPM), Low-Noise, Blue-Sensitive (Rev. 9). (2022). Onsemi. <https://www.onsemi.com/pdf/datasheet/microc-series-d.pdf>
21. AND9809/D: Reference Designs for the SMA and SMTPA MLP-Packaged SiPM Evaluation Boards (Rev. 3). (2024). Onsemi. <https://www.onsemi.com/pub/Collateral/AND9809-D.PDF>
22. Time-to-Digital Converter IP-Core for FPGA at state of the art. (2021). IEEE Journals & Magazine | IEEE Xplore. <https://ieeexplore.ieee.org/document/9452098>
23. Hackster.io. (2021, April 18). 4 channel TDC (Time Digital Converter) on CMOD A7 35T. <https://www.hackster.io/zhoumingxiang/4-channel-tdc-time-digital-converter-on-cmod-a7-35t-33429a>
24. Basys 3 AMD ArtixTM 7 FPGA Trainer Board: Recommended for introductory users. (n.d.). Digilent. <https://digilent.com/shop/basys-3-amd-artix-7-fpga-trainer-board-recommended-for-introductory-users/>
25. ADS7028 Small, 8-Channel, 12-Bit ADC with SPI Interface, GPIOs, and CRC. (2020). Texas Instruments. <https://www.ti.com/lit/ds/symlink/ads7028.pdf>
26. Wikipedia contributors. (2025, September 20). Minimum chi-square estimation. Wikipedia. https://en.wikipedia.org/wiki/Minimum_chi-square_estimation
27. Blobel, V. (n.d.). Data fitting [Slide show]. University of Hamburg. https://www.desy.de/~sschmitt/blobel/blobel_fitting.pdf
28. Allison, J., Amako, K., Apostolakis, J., Arce, P., Asai, M., Aso, T., Bagli, E., Bagulya, A., Banerjee, S., Barrand, G., Beck, B., Bogdanov, A., Brandt, D., Brown, J., Burkhardt, H., Canal, P., Cano-Ott, D., Chauvie, S., Cho, K., . . . Yoshida, H. (2016). Recent developments in Geant4. Nuclear Instruments and Methods in Physics Research Section a Accelerators Spectrometers Detectors and Associated Equipment, 835, 186–225. <https://doi.org/10.1016/j.nima.2016.06.125>
29. Agostinelli, S., Allison, J., Amako, K., Apostolakis, J., Araujo, H., Arce, P., Asai, M., Axen, D., Banerjee, S., Barrand, G., Behner, F., Bellagamba, L., Boudreau, J., Broglia, L., Brunengo, A., Burkhardt, H., Chauvie, S., Chuma, J., Chytracek, R., . . . Zschiesche, D.

- (2003). *Geant4—a simulation toolkit. Nuclear Instruments and Methods in Physics Research Section a Accelerators Spectrometers Detectors and Associated Equipment*, 506(3), 250–303. [https://doi.org/10.1016/s0168-9002\(03\)01368-8](https://doi.org/10.1016/s0168-9002(03)01368-8)
30. Allison, J., Amako, K., Apostolakis, J., Araujo, H., Dubois, P. A., Asai, M., Barrand, G., Capra, R., Chauvie, S., Chytracek, R., Cirrone, G., Cooperman, G., Cosmo, G., Cuttone, G., Daquino, G., Donszelmann, M., Dressel, M., Folger, G., Foppiano, F., . . . Yoshida, H. (2006). *Geant4 developments and applications*. IEEE Transactions on Nuclear Science, 53(1), 270–278. <https://doi.org/10.1109/tns.2006.869826>
31. Komori, H., & Mitsui, K. (1981). *Energy spectrum of cosmic-ray muons. Il Nuovo Cimento C*, 4(1), 52–74. <https://doi.org/10.1007/bf02507746>
32. Kuo, Y.-H. (2010). *Determination of the Angular Distribution of Cosmic Rays at Sea Level*. MIT. <https://dspace.mit.edu/bitstream/handle/1721.1/61208/701107722-MIT.pdf>

IV

Appendices

Appendix A

A Special relativity

According to the laws of physics, an object cannot travel faster than the speed of light. However, in some cases these laws do not seem to apply, as some objects can travel a larger distance than light would have in the same time.

An example of this are muons, having a look at their mean lifetime and the height at which they are most commonly formed, it looks like there is no way that they can reach the earth. Even though it looks like that the laws of physics do not apply in this case, they still do. At objects travelling close to the speed of light, a phenomenon called time dilation applies.

A.1 Mass-energy relation

As stated earlier, an object cannot travel faster than the speed of light. But why is this actually the case?

Normally, we would use the mass-energy relation formula to calculate the energy of a particle. [1]

$$E = mc^2 \quad (1)$$

However, this equation only applies in a system's rest frame, when a particle has zero velocity. When a particle has velocity, its energy increases. So in order to account for a particle's velocity, we use the following formula

$$E = \gamma mc^2 \quad (2)$$

The γ symbol in equation 4 is the Lorentzfactor. This factor describes the time dilation in Einstein's theory of relativity. The Lorentzfactor (γ) is defined as [1]

$$\gamma = \frac{1}{\sqrt{1 - (\frac{v}{c})^2}} \quad (3)$$

A.2 Lorentzfactor

In order to derive the Lorentzfactor, we assume the fact that the speed of light is a constant in each reference frame.

Imagine 2 mirrors facing opposite of each other, as seen in figure 3. These mirrors are both moving in the same direction, and our inertial frame is moving along with the mirrors, thus it looks like the mirrors are standing still and the light moves directly up and down.

Given an external clock, the time between ticks is Δt . The time it takes for the light to travel from A to B is one clock tick, or Δt , and another to travel back from B to A.

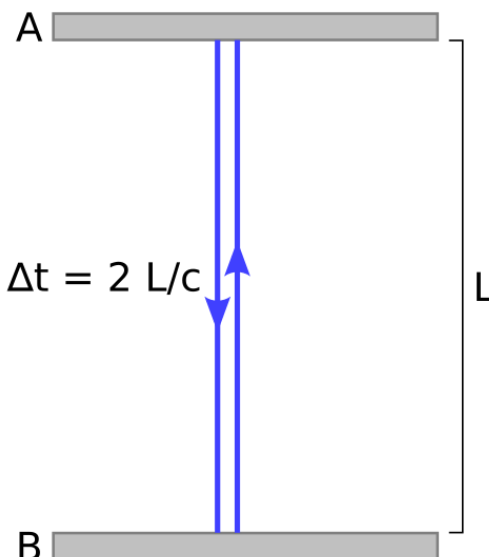


Figure A.1: Observer at rest measures time $2L/c$ between co-local events of light signal generation at A, to B and arrival back at A. (Source: [2])

In this scenario, we define the distance between the two mirrors as L . In order to calculate the time it takes for light to travel

between the two mirrors, we can use a rewritten version of the standard formula for velocity.

$$t = \frac{s}{v} \quad (6)$$

The light travels back and forth between the mirrors, so the total distance is $2L$. The light travels at the speed of light (c), so we can define the time between clock ticks as the following:

$$\Delta t = \frac{2L}{c} \quad (7)$$

If we look at this scenario from a different frame of reference, one outside the inertial frame, the total observed travelled distance will be larger, as can be seen in Figure 4.

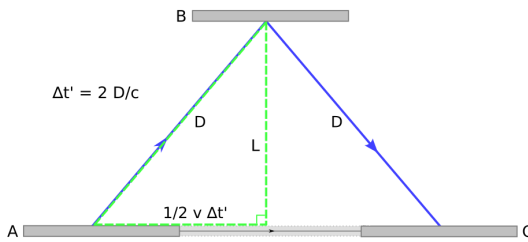


Figure A.2: Events according to an observer watching as the mirror setup moves to the right, with the measured time being $2D/c$ between light signal generation at A, to Band arrival back at A. (Source: [3])

In this case, $\Delta t'$ is the time between clock ticks from the perspective of the external reference frame, which is then defined as follows according to Figure 3:

$$\Delta t' = \frac{2D}{c} \quad (8)$$

The total horizontal length can then be defined using a rewritten version of (6) and, because we only want the distance from one mirror to the same axis as the second mirror, we divide it by two (9'). And the travelling time (t) is equal to $\Delta t'$, which results in (9).

$$s_{half} = \frac{1}{2} vt \quad (9')$$

$$s_{half} = \frac{1}{2} v \Delta t' \quad (9)$$

In order to calculate the distance (D) from one mirror to the other, we use the Pythagorean theorem, with the sides L and (9), resulting in the following equation.

$$D = \sqrt{\left(\frac{1}{2} v \Delta t'\right)^2 + L^2} \quad (10)$$

If we then substitute this in (8) and rewrite it so that $\Delta t'$ is only on the left side, we get (11'). Then, after substituting (7), we get the following.

$$\Delta t' = \frac{2}{c} \sqrt{\left(\frac{1}{2} v \Delta t'\right)^2 + L^2}$$

$$(\Delta t')^2 = \frac{4}{c^2} \left(\frac{1}{4} v^2 (\Delta t')^2 + L^2 \right)$$

$$(\Delta t')^2 = \frac{v^2 (\Delta t')^2}{c^2} + \frac{4L^2}{c^2}$$

$$(\Delta t')^2 - \frac{v^2 (\Delta t')^2}{c^2} = \frac{4L^2}{c^2}$$

$$(\Delta t')^2 \left(1 - \frac{v^2}{c^2}\right) = \frac{4L^2}{c^2}$$

$$(\Delta t')^2 = \frac{4L^2}{c^2 \left(1 - \frac{v^2}{c^2}\right)} \quad (11')$$

$$\Delta t' = \frac{2L}{c \sqrt{1 - \left(\frac{v}{c}\right)^2}} \quad (11)$$

If we have a closer look at this formula, we can see that it contains the Lorentzfactor (5). Substituting this into our formula, we get the final equation.

$$\Delta t' = \frac{1}{\sqrt{1 - \left(\frac{v}{c}\right)^2}} \Delta t \quad (12')$$

$$\Delta t' = \gamma \Delta t \quad (12)$$

As we can see, the time between ticks from the external inertial frame is longer. Thus, time appears to be moving slower in the second

situation. This explains why objects, that are travelling close to the speed of light, can travel longer distances than light itself can, as their time appears slower than our time.

A.3 Characteristics of the Lorentzfactor

In order to explain why objects cannot travel faster than the speed of light, we have to examine the effects of the Lorentzfactor on an object's energy.

If we write the Lorentzfactor equation as a function, we get the following.

$$\gamma(v) = \frac{1}{\sqrt{1-(\frac{v}{c})^2}} \quad (4)$$

If we plot this function, where v approaches the speed of light (c), we get Figure 1.

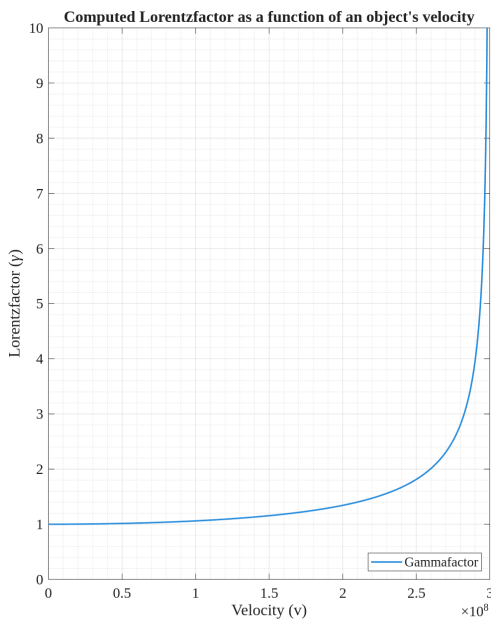


Figure A.3: The computed Lorentzfactor as a function of an object's velocity, where the velocity approaches c .

Looking at Figure 1 and (4), we can determine the following characteristics for the function.

$$\text{Range}(\gamma) = [1, \infty) \quad (5)$$

$$\lim_{v \rightarrow c} \gamma(v) = \infty \quad (6)$$

A.4 Conclusion

Applying the knowledge of the characteristics of the Lorentzfactor to the aforementioned mass-energy relation equation (2), tells us that when an object travels at a velocity that approaches c , the Lorentzfactor approaches infinity, as shown in the following equation.

$$E = \lim_{v \rightarrow c} (\gamma(v) \cdot mc^2)$$

$$E = \lim_{v \rightarrow c} (\gamma(v)) \cdot mc^2 \quad (7)$$

The limit in this equation is the same as (6), thus we can see that an object needs to have infinite energy in order to travel at c , which is physically impossible.

So Newton's idea of mechanics falls apart at higher speeds. And this is when we use Einstein's theory of relativity, which explains movements of objects at relativistic speeds, or in other words, speeds close to the speed of light.

A.5 References

1. Bouwens, R. E. A., Kranendonk, W., Van Lune, J. P., Prop - van Den Berg, C. M., Van Riswick, J. A. M. H., & Westra, J. J. (2022). *Binas: Informatieboek havo / vwo voor het onderwijs in de natuurwetenschappen* (7de editie). Noordhoff Uitgevers.
2. Mdd4696. (2006, 8 januari). *File:Time-dilation-001.svg* - Wikimedia Commons. <https://commons.wikimedia.org/wiki/File:Time-dilation-001.svg>
3. Mdd4696. (2006, januari 13). *File:Time-dilation-002.svg* - Wikimedia Commons. <https://commons.wikimedia.org/wiki/File:Time-dilation-002.svg>

Appendix B

B Cosmic Watch

The Cosmic Watch is a desktop muon detector capable of detecting muons. It originated from MIT, a well-known university and research facility. Recently, the development has been taken over by the University of Delaware, which has designed the latest version (V3), which this analysis is about. [1]

The schematics and PCB designs of the Cosmic Watch are public, and we will thus be referencing them multiple times when analysing the various electronic circuits. The firmware, however, is not publicly accessible, thus we will not be discussing that here.

B.1 Principle of operation

The Cosmic Watch is built around a scintillator plate [^2.4] along with a SiPM [^2.5.3] as the sensor. This setup is capable of detecting single muon interactions, as well as calculating the amount of emitted photons by the scintillator.

To suppress background noise and false readings, the Cosmic Watch supports coincidence detection using multiple units. When two detectors are connected to each other, they will compare events. When two events happen at both detectors simultaneously, it counts as a coincidence detection.

B.2 Scintillator and photon detection

The part of the detector that actually detects the muons, is the SiPM. The detector uses a $50 \times 50 \times 10\text{ mm}$ plastic scintillator plate, along with the Onsemi MICROC-60035-SMT-TR SiPM sensor [2]. The sensor is optically coupled to the scintillator plate with optical gel and/or a silicone pad.

Finally, this construction is wrapped in aluminium foil and black electrical tape, to optically isolate the SiPM from outside light. By wrapping the plate in aluminium foil, the chance that a particle, that is not a muon, passes through and interacts with the plate, is greatly reduced.

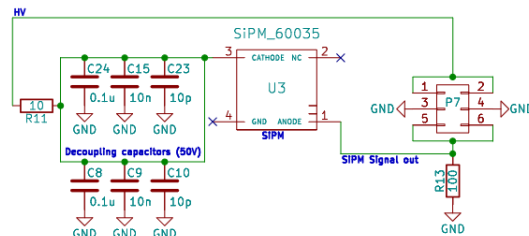


Figure B.1: SiPM circuit diagram of the Cosmic Watch. (Source: [3])

The circuit that houses the SiPM is actually relatively simple, it basically consists of three components, the SiPM itself, a set of decoupling capacitors and the connector to the main board. (Figure B.1)

The set of decoupling capacitors are used to filter out input noise on the SiPM input voltage from the power supply, as the tiniest amount of interference can mess with the accuracy of the sensor.

Also note the importance of the pull-down resistor (R13), this resistor will ensure that the voltage at the anode of the SiPM is pulled low,

so when the SiPM is not detecting anything, the output signal always returns to 0 V.

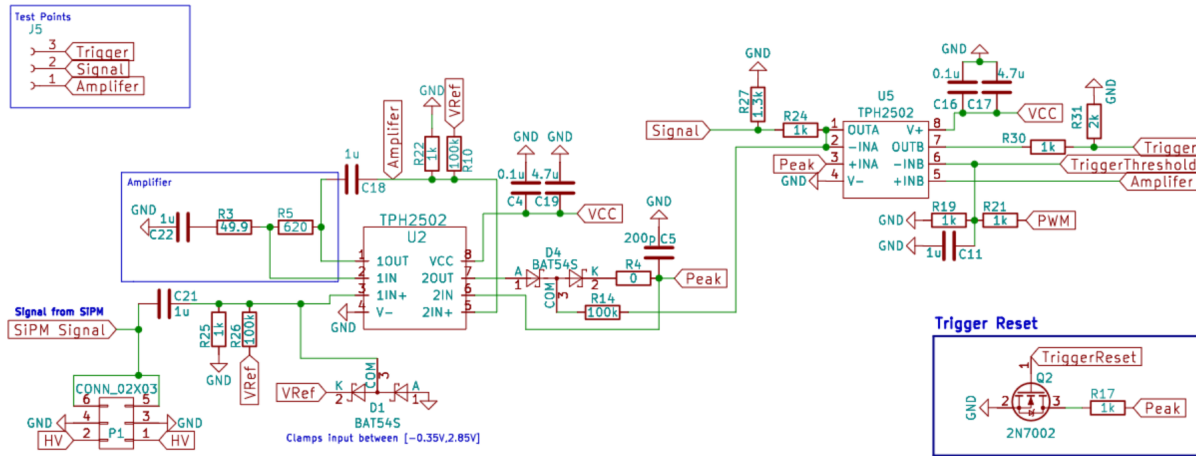


Figure B.2: Amplifying, Triggering and Peak Detecting circuits diagram of the Cosmic Watch. (Source: [\[3\]](#))

B.3 Amplifying, Triggering and Peak Detecting circuits

The signal coming from the SiPM sensor is far too small to measure with the Raspberry Pi Pico MCU. That is why it is necessary to amplify the signal before trying to measure anything.

The duration of the pulse from the SiPM is also too short for the MCU to measure. In order to be able to measure it, the peak voltage coming from the sensor is stored in a capacitor for a longer duration for the MCU to sample. This is what the triggering and peak detecting circuits are used for; they hold the peak voltage and trigger the MCU to sample that voltage.

The first amplification stage is handled by the right side of the TPH2502 (U2) Dual operational amplifier; the pins labelled with a 1. (Figure B.2) This amplifies the SiPM signal from the microvolts to millivolts range.

The various other resistors and capacitors, are used to bias the op-amp and the Schottkydiodes at D1 are used to clamp the input between 0 V (GND) and 2.5 V (VRef).

The amplified output signal then splits to two separate other stages: the peak detection stage and the triggering stage.

The peak detection stage is in the middle of the diagram. (Figure B.2) This stage is responsible for capturing the pulse of the SiPM signal and holding this peak for a longer duration, so that the relatively slow microcontroller has enough time to sample the signal.

In simple terms, the capacitor (C5) is charged by the SiPM signal and will hold that voltage for a certain amount of time.

This peak voltage then gets fed into another TPH2502 opamp which further amplifies the peak signal so that it can be properly consumed by the microcontroller's ADC.

The trigger reset circuit is also part of this stage, when the TriggerReset line, which is connected to the microcontroller, is pulled high, a MOSFET triggers, shorting the peak line to GND, and thus discharging C5 and resetting the system for the next measurement.

The last part of this circuit is the triggering stage. This stage is used to trigger the microcontroller to read the signal. It gets

activated when the first amplification stage outputs a signal, in turn triggering the microcontroller to sample the voltage that is stored in the capacitor.

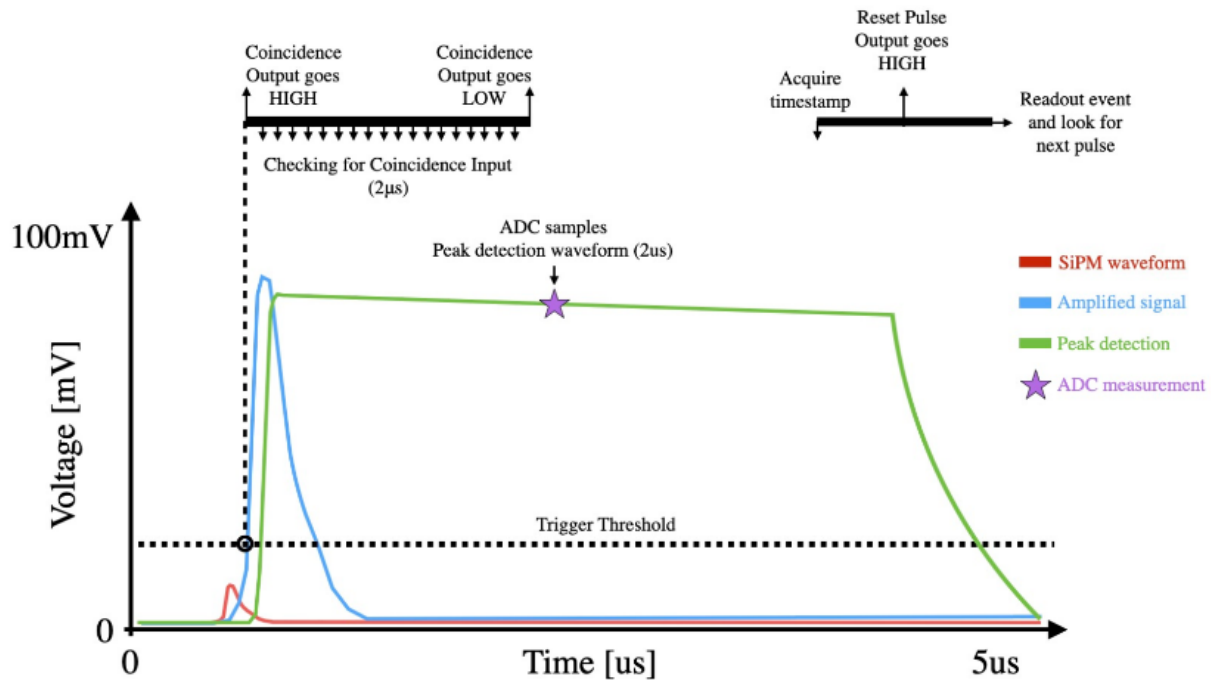


Figure B.3: A description of the analogue circuitry and CPU routine. The SiPM pulse (red) is amplified (blue), and peak detected (green). When the amplified pulse crosses the trigger threshold (software defined voltage level), it triggers the detector to 1) check for coincidence signal from the coincident detector, 2) samples the amplitude of the peak detector waveform, and 3) takes a time stamp and reads out the event information. (Source: [\[4\]](#))

B.4 Event cycle

Putting all of these circuit together, the detector is capable of detecting small pulses from the SiPM and amplifying them to be sampled by the microcontroller's ADC.

The whole cycle for a given event is illustrated in the diagram above. (Figure B.3) This diagram gives us a rough idea of what the analogue signals of the various stages look like. These signals can also be probed and connected to an oscilloscope by using the three test points (J5) on the Cosmic Watch.

The cycle starts when the SiPM detects an interaction, and thus outputs a small voltage proportional to the amount of photons that

were measured. This is the peak of the red line in the graph. (Figure B.3)

When this signal reaches the main board, it is amplified by the amplifying circuit. This is the peak of the blue line in the graph. (Figure B.3)

This amplified signal then gets captured by the peak detecting circuit and gets stored in the capacitor. The green line in the graph represents this stage. (Figure B.3)

After about 2 μs, the MCU is notified by the triggering circuit, and samples the voltage of the peak using the MCU's built-in ADC.

Lastly, the timestamp of the event is acquired by the MCU and the TriggerReset line (Figure B.2) is pulled high, resetting the system. [\[4\]](#)

B.5 Other circuits

B.5.1 DC-DC Booster

The SiPM requires a low ripple, stable overvoltage above the breakdown voltage ($V_{br} = 24.5 V \pm 0.2$). A higher overvoltage enhances the sensor's gain and photon detection efficiency. In this case the MAX5026 DC-DC Booster was used, which is suitable for providing a stable, low-ripple voltage of 30.0 V. [5]

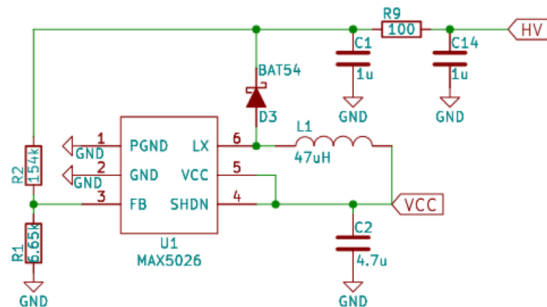


Figure B.4: DC-DC Booster circuit diagram of the Cosmic Watch. (Source: [3])

Along with this IC, the DC-DC Booster circuits also feature some decoupling capacitors, to further lower the ripple. (Figure B.4)

B.6 References

1. *CosmicWatch: The Desktop Muon Detector (V3X)*. (n.d.). <https://arxiv.org/html/2508.12111v1>
2. *Silicon Photomultipliers (SiPM), Low-Noise, Blue-Sensitive C-Series SiPM Sensors*. (2022). Onsemi. <https://www.onsemi.com/pdf/datasheet/microc-series-d.pdf>
3. Spenceraxani. (n.d.). *CosmicWatch-Desktop-Muon-Detector-v3X /PCB/Circuit_Diagram.pdf*. GitHub. https://github.com/spenceraxani/CosmicWatch-Desktop-Muon-Detector-v3X/blob/50adc8806ca86587977e0223ad46905fed3c06e/PCB/Circuit_Diagram.pdf
4. Spenceraxani. (n.d.). *CosmicWatch-Desktop-Muon-Detector-v3X /The_Instruction_Manual.pdf*. GitHub. <https://github.com/spenceraxani/CosmicWatch-Desktop-Muon-Detector-v3X/blob/50adc8806ca86587977e0223ad46905fed3c06e/The%20Instruction%20Manual.pdf>

5. *MAX5025–MAX5028: 500kHz, 36V Output, SOT23, PWM Step-Up DC-DC Converters*. (2009). Maxim Integrated Products. <https://www.analog.com/media/en/technical-documentation/data-sheets/MAX5025-MAX5028.pdf>

Appendix C

C Muon trajectory detectors

Besides measuring the mere existence of muons, some muon detectors are also capable of measuring the trajectory of the muons. There have been multiple projects that have focussed on measuring this trajectory.

One of these projects was done by students at the University of Exeter. [1] The aim of their project was to create a setup that was capable of muon tomography, which can be used to image large objects and geographical structures. They have made a video about their findings and early prototypes, but as far as we know, they never finished the detector.

Another detector, that was capable of measuring muon trajectory, was made by students at Texas A&M University. They have also made a video about the detector, which actually shows a working prototype, along with them sharing their plans for future additions. [2]

C.1 Principle of operation

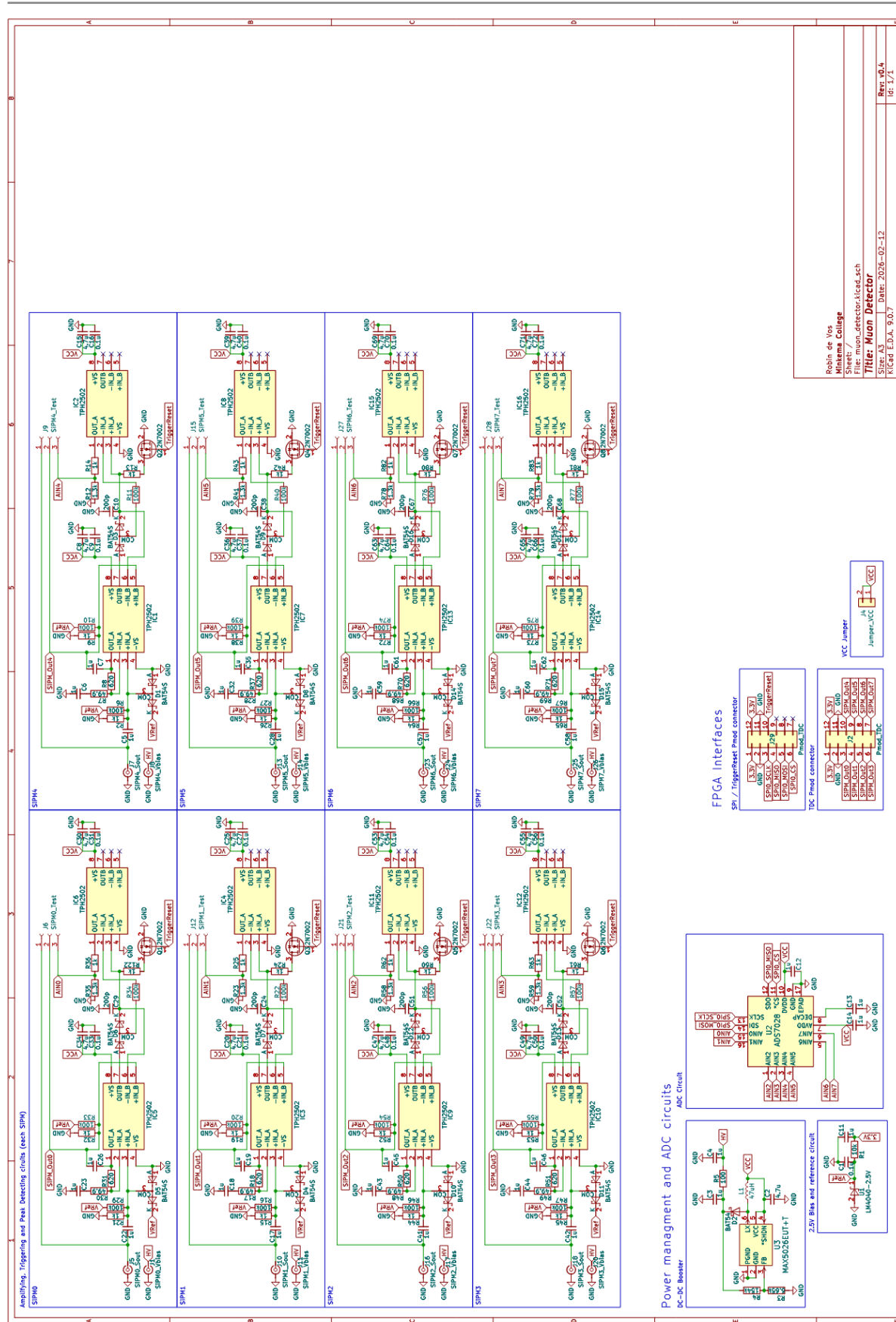
Both of these detectors work based on the same principles. They make use of a large scintillator plate with a SiPM sensor at each of the corners of the plate. Then, based on the time and voltage differences at each sensor, they determine the impact position in the plate using triangulation.

When two or more of these plates are stacked above each other, you can calculate the muon's trajectory based on the difference of the position of the plates. When these plates are placed at a sufficient distance from each other, the velocity of the muons can also be roughly estimated.

C.2 References

1. Katie Hinton. (2018, 13 december). *Muon detecting* [Video]. YouTube. <https://www.youtube.com/watch?v=uS8TC29xkns>
2. TAMU Discover, Explore & Enjoy Physics. (2024, 19 september). *Giant Muon Detector (Ryan Mueller's Group)* [Video]. YouTube. <https://www.youtube.com/watch?v=W6TyWHI7JQ>

Appendix D



Appendix E

E Schematic BOM

Item	Name	Count	Generic name	Cost
1	1K resistor	32	RES SMD 1K OHM 1% 1/8W 0805	0.21
2	1.3K resistor	8	RES SMD 1.3K OHM 1% 1/8W 0805	0.64
3	100 Ohm resistor	1	RES SMD 100 OHM 1% 1/8W 0805	0.08
4	10k Ohm resistor	1	RES SMD 10k OHM	0.08
5	154k resistor	1	RES SMD 154k OHM 0.1% 1/8W 0603	0.19
6	6.65k resistor	1	RES SMD 6.65k OHM 0.1% 1/8W 0603	0.08
7	100k resistor	24	RES SMD 100k OHM 1% 1/8W 0805	0.22
8	49.9 Ohm resistor	8	RES SMD 49.9 OHM 1% 1/8W 0805	0.72
9	620 Ohm resistor	8	RES SMD 620 OHM 1% 1/8W 0805	0.64
10	4.7 uF capacitor	17	CAP CER 4.7UF 50V X7R 0805	1.46
11	1 uF capacitor	30	CAP CER 1UF 50V Y5V 0805	1.56
12	0.1 uF capacitor	17	CAP CER 0.1UF 50V X7R 0805	0.09
13	200pF capacitor	8	CAP CER 200pF 50V Y5V 0805	0.64
14	LM4040 2.5V	1	IC VREF SHUNT 0.5% SOT23	0.42
15	47uH inductor	1	FIXED IND 47UH 190MA 4.86OHM SMD	0.13
16	2N7002 transistor	8	MOSFET SOT23 N 60V 5OHM 150C	0.64
17	TPH2502 Op amp	16	IC OPAMP 2 CIRCUIT	14.72
18	MAX5026 DC-DC booster	1	IC REG BOOST ADJ 260MA SOT6	1.60
19	BAT54WS Schottky diode	1	DIODE SCHOTTKY 30V 200MA SOD323	0.13
20	BAT54S Schottky diode	16	DIODE ARR SCHOT 30V 200MA SOT233	2.08
21	SMA connector	16	SMA PCB MOUNT RA JACK	25.87
22	ADS7028 adc	1	IC ADC 12BIT SAR 16WQFN	5.50
23	Pmod connector	2	CONN HEADER R/A 16POS 2.54MM	4.58
24	2x1 header	1	CONN HEADER VERT 2POS 2.54MM	0.08
Total				62.36